Spacelab Experiment Definition Study
on
Phase Transition and Critical Phenomena in Fluids
Interim Report on Experimental Justification

by

M.R. Moldover and R.J. Hocken
National Bureau of Standards, Washington, D. C. 20234

and

R.W. Gammon and J.V. Sengers
National Bureau of Standards, Washington, D. C. 20234

and

Institute of Molecular Physics, University of Maryland
College Park, MD 20742

TABLE OF CONTENTS

SUMMARY

Important scientific questions concerning pure fluids and fluid mixtures near critical points are identified and are related to the progress of several disciplines. Consideration is given to questions about thermodynamic properties, transport properties, and the complex nonlinear phenomena which occur when fluids undergo phase transitions in the critical region. We discuss, quantitatively, the limitations to answering these questions by experiments in the earth's gravitational field. The distinction is made between practical limits which may be extended by advances in technology and intrinsic ones which arise from the modification of fluid properties by the earth's gravitational field. The kinds of experiments near critical points which could best exploit the low gravity environment of an orbiting laboratory are identified. These include studies of the index of refraction, constant volume specific heat, and phase separation.

Key words: Critical point; gravity effects; phase transitions.

1. **Phase Transition and Critical Phenomena in Fluids: Scientific Questions and Interactions with Other Disciplines.**

   1.1 **Introduction**

   The justification for space experiments in the area of "Phase Transition and Critical Phenomena in Fluids" is essentially scientific. This particular area of science has strong interactions with solid state physics, fluid physics and other areas of physics. We may expect that scientific advances in these areas will bring, indirectly, long term technological and economic benefits; however, it cannot be said that the space experiments in themselves will produce such benefits. Therefore the justification for space experiments in phase transition and critical phenomena in fluids depends upon first establishing that this is an important, active field of scientific research and secondly, upon establishing that space experiments are likely to have a major impact on its further development. A large part of the importance of this area of research results from its initimate relationship to many areas of solid state science. This will be discussed in the next section. In order to develop a rationale for the argument that space experiments can have a major impact in this area of research, we first discuss the important unanswered questions on the subject; we then describe how gravity imposes severe limitations in finding experimental answers to these questions; and, finally, we indicate to what extent these limitations can be reduced by conducting experiments in space.

1.2 The Relationship of "Phase Transition and Critical Phenomena in Fluids" to other Disciplines.

Many of the research subjects described as included in research on "phase transition and critical phenomena in fluids" are intimately related to similar subjects in solid state physics. The experimental phenomena observed and the theoretical ideas used to describe both fluids and solids have a high degree of overlap. Indeed, this overlap is recognized by the "Physics and Astronomy Classification Scheme, 1975" adopted by the Abstracting Board of the International Council of Scientific Unions. This classification scheme, which is used for grouping scientific articles for publication and information retrieval, groups "phase equilibria, phase transitions and critical points" together for both solid and fluid systems. We expect that important experiments on fluid systems, such as those to be defined in this study, will have a substantial impact on corresponding areas of solid state science. The basis for our expectation is the strong interrelationship in recent history between the study of phase transition and critical phenomena in fluid and in solid systems. The interrelationship arises from analogies between many phenomena which occur near the critical point of the liquid-gas phase transition in pure fluids and phenomena which occur at a corresponding "critical point" of phase transitions in very different kinds of physical systems. A list of these different kinds of physical systems would include ferromagnets near the Curie point, anti-ferromagnets near the Néel point, certain ferroelectrics near the ferro-electric-paraelectric phase transition, alloys exhibiting order-disorder transitions (e.g. β-brass), crystals exhibiting order-disorder structural transitions (e.g. ammonium chloride), binary liquid mixtures near consolute points, multicomponent fluid mixtures near plait points, and helium near its

superfluid transition. (For general references on these subjects see: Elcock, 1956; Stanley, 1971; Heller, 1967; Fisher, 1967).

In each of these physical systems, there is a "quality" (such as the difference between the densities of the liquid and vapor phases of. a fluid) which distinguishes between two phases which coexist in thermodynamic equilibrium. As the critical point is approached this quality gradually disappears. The gradual disappearance of this quality is the most obvious feature which distinguishes phase transitions with critical points from other sorts of phase transitions such as melting, sublimation, or crystallographic phase changes.

The diverse physical systems with critical points have a number of experimental properties in common near their respective critical points. They all exhibit a specific heat anomaly, long thermal relaxation times, a marked sensitivity to external fields and impurities, and the quality which is disappearing shows large long-lived fluctuations. The density fluctuations in a pure fluid are responsible for the striking visual effects called critical opalescence. Analogous fluctuations in solid systems manifest .hemselves in ways such as enhanced neutron scattering, ultrasonic attenuation, and electrical resistivity.

The existence of diverse physical systems displaying analogous critical phenomena provides the experimenter with the opportunity to choose both the best material and the best technique for studying one or another aspect of critical phenomena. For example, the size of fluctuations is rather easily studied in magnetic solids with neutron scattering, even very far from the critical point. The same technique cannot be used extremely close to the critical point because the fluctuations become much larger than the wavelength of the neutrons available. On the other hand, fluctuations in fluids may be

4

studied easily quite close to the critical point using scattered light. We wish to emphasize that extremely close (often near 99.9% of the critical temperature) to critical points, all experiments on solids are limited by lattice strains which result from impurities, vacancies, etc. Thus experiments with fluids (which continuously "anneal" themselves) offer the best opportunities for closest approach to the critical point.

Since critical phenomena occur in a wide range of systems, one might expect that their theoretical explanation does not depend upon the detailed nature of the interatomic forces in each system but rather, c·ld be based upon an accurate treatment of interactions which contain only those few general properties of the true interatomic forces which are needed to make critical points occur. Accordingly, similar theoretical treatments of microscopic interactions have been used to interpret data on these diverse systems. The van der Waals model of a fluid, molecular field model of a ferromagnet, and the Bragg-Williams model of a binary alloy are closely related in approach and yield similar predictions concerning thermodynamic properties near the critical point of each of the corresponding systems. There is an exact correspondence between the lattice gas model of a fluid and the Ising model of a ferromagnet. This correspondence has been exploited as a plausibility argument for taking a wide variety of theoretical results based on lattice models of critical phenomena and applying them to describe real fluids as well as real solids near critical points. Interestingly, several important recent advances in the theory of lattice models are outgrowths of the "renormalization group" technique, a technique developed for problems in theoretical high energy physics (Ma, 1973).

5

Other aspects of phase transition phenomena in liquids have solid state counterparts. Away from the critical point itself, phase transitions in both fluids and solids may be initiated by nucleation processes or may occur spontaneously through a spinodal decomposition mechanism. The theoretical description of these processes make use of the concepts of interfacial energy, bulk free energy, and diffusion. The concepts are applicable to both fluid and solid systems. The time scales for phase changes are very different for fluid and solid systems, thus facilitating complementary experimental studies which benefit the understanding of both fluids and solids. (Cahn, 1968; Langer and Bar-on, 1973; Schwartz et al., 1975).

In summary, basic scientific studies of phase transitions and critical phenomena in fluids are closely related to the study of similar phenomena in solid systems. It is also quite likely that future developments in chemical engineering will exploit the progress now being made in the understanding of thermodynamic and transport properties of fluids near critical points. In the study of pure fluids, equations of state for the critical region have been developed recently which are much more accurate representations of data than are standard engineering equations. (Levelt Sengers et al. 1976). These new representations have very few parameters which must be adjusted for each fluid; thus, they require fewer experimental measurements for reliable predictions. The extension of these new equations to special mixtures has been demonstrated and work on extending them to mixtures of engineering interest is in progress. (Leung and Griffiths, 1973; D'Arrigo et al., 1975). Similar advances have occurred and are occurring in the correlation and prediction of transport properties in the critical region. Thus we can expect that advances in the scientific understanding of phase transition and critical phenomena in fluids will influence chemical engineering practice.

6

1.3 Important Questions in Phase Transition and Critical Phenomena in Fluids.

We will consider some of the important scientific questions in the area of phase transition and critical phenomena in fluids which are amenable at least to a partial answer by experiment. Naturally this cannot be done without some reference to current theoretical ideas. We will first discuss pure fluids and then fluid mixtures. Perhaps the single most important question in this area is: exactly how much alike are the superficially analogous phenomena occurring in the large variety of systems showing critical points? Rigorous renormalization group calculations which apply to large classes of model systems indicate that static correlation functions and all the thermodynamic properties (each of which can of course be calculated from the correlation functions) are "universal" (in the sense that the same description applies to each) asymptotically close to the critical point. More specifically, they predict that the correlation functions will depend upon the dimensionality of the system under consideration (e.g. whether it is two dimensional like a membrane or three dimensional like a crystal) and the dimensionality of the "order parameter" (or the "quality" which vanishes as phases become identical at the critical point). Thus the correlation functions for a fluid (where the order parameter is the scalar difference in density between coexisting phases) will differ from correlation functions for isotropic magnets (where the order parameter is a three-dimensional vector). (Wilson and Kogut, 1974).

Variables such as the lattice structure (e.g. hexagonal close-packed or cubic) and the presence or absence of second nearest neighbor interactions etc. are expected to be irrelevant in determining the functional

7

form of the asymptotic expansions of correlation functions and thermodynamic functions; however these other variables will determine the numerical value of the critical temperature itself and numerical values of various amplitudes in the expansions for correlation and thermodynamic functions. At the present time, nearly all thermodynamic experiments on pure simple fluids indicate small, but experimentally significant, differences between the measured properties and those calculated for three dimensional lattice models with a scalar order parameter. (Levelt Sengers and Sengers, 1977). It is possible that these differences indicate that fluids do not belong to the same "universality" class as the lattice models with a scalar order parameter. It is also possible these differences indicate that the amplitudes of the corrections to asymptotic behavior are quite different for fluids than for the lattice models studied. An experimental distinction between these two possibilities would be of great value in understanding the range of applicability of this important idea of universality. It is possible that this distinction could be made by measurements of thermodynamic properties closer to the critical point than is now possible in experiments carried out in the earth's gravitational field. The very same situation exists to a lesser degree when different pure fluids are intercompared. The apparent differences between fluids are smaller (hence subject to greater experimental uncertainties) than the differences between fluids as a class and lattice models; however, the same question exists regarding their origin. Again, the answer could result from experiments carried out closer to the critical point than presently possible.

The decay of the range of density fluctuations (or the pair correlation length) may be measured by measuring the angular distribution of light, X-rays, or neutrons scattered by a fluid. The temperature and density dependence of this quantity is predicted to be universal, but a significant

8

test of universality cannot be made until two conditions are met: 1) The wavelength of the incident radiation must be short compared with the range of correlation. 2) The wavelength of the incident radiation must be long · · red with the range of the interatomic forces. Neutron and X-ray scatter ·ₛ experiments easily satisfy the first criterion; however, the second criterion is not well satisfied in present experiments. Thus, a somewhat arbitrary separation of the observed scattering into a part due to critical fluctuations and a part due to short range order in the fluid is now required prior to a test of the predictions of universality (as defined above). The best experiments to date seem to indicate significant differences between the predictions of lattice models and the behavior of real fluids (Warkulwiz et al., 1974; Lin and Schmidt, 1974). Experiments with scattered light are now unable to satisfy the criterion mentioned above that the wavelength be much smaller than the correlation length. The correlation length increases rapidly as the critical point is reached. In a low gravity environment, the critical point could be approached much closer than is now possible; thus a much tighter test of this aspect of universality will be possible.

Other questions which may be answered by experiments defined within this study pertain more specifically to aspects of fluid dynamics and structure. Hence the answers are less likely to have as broad an impact on condensed matter science than would a clear answer to the question of universality. Nevertheless, the properties of fluids are sufficiently alike at critical point, that questions about large classes of fluids may be answered with an experiment on one or two fluids.

Questions of considerable interest are: What is the nature of the small anomalies which occur in the viscosity (Sengers, 1973), dielectric constant

9

(Hartley et al., 1974), refractive index (Hocken and Stell, 1973; Stell and Hoye, 1974; Bedeaux and Mazur, 1973), and diameter of the coexistence curve (Weiner et al., 1974) (i.e. the average of the liquid and vapor densities) as the critical point is approached? There are theoretical and experimental controversies on the nature of the anomaly for each of these properties. It is reasonable to believe that the more definitive experimental results available from low-g experiments would have a significant impact on the theories for these properties in fluids. The experimental nature of the stronger critical point anomalies in sound attenuation (Thoen and Garland, 1974) and thermal conductivity (Sengers, 1973) is somewhat better understood from earth based experiments, hence, low-g environments are less likely to have an impact on the theory of these properties.

The dynamics of the process of macroscopic phase change in pure fluids is poorly understood in the vicinity of the critical point. A variety of questions remain to be answered. We will briefly mention a few. There is least one observation which suggests standard nucleation theories are fundamentally wrong near the critical point in pure fluids (Huang et al., 1975). Is this observation correct? Other earthbound experiments are necessary in this area, but only in a low gravity environment will it be possible to obtain a homogeneous, macroscopic volume of a fluid under conditions sufficiently close to critical to yield a definitive study of this problem. The spinodal decomposition mechanism of phase separation occurs in alloys, glasses, and binary liquid mixtures (Schwartz et al., 1975). Does this process occur in pure fluids? If it does, it is quite likely that the study of spinodal decomposition in pure fluids (where many of the macroscopic parameters of the theory are well understood) will clarify the understanding of spinodal

10

decomposition in these other kinds of systems. Are there critical point anomalies in the process of bubble and droplet growth (or evaporation and condensation)? Do they influence the time of equilibration of macroscopic two-phase samples of pure fluids as has been suggested in two public tions? (Dahl and Moldover, 1972; Brown and Meyer, 1972). What will be the dominant mechanisms for macroscopic phase separation upon cooling a pure fluid below the critical point if bouyant forces on bubbles and droplets are greatly reduced? Many other questions are possible in this poorly understood area of phase separation.

In fluid mixtures, important scientific questions analogous to the ones above exist. Specifically, the question: Do real fluid mixtures have the same "universal" thermodynamic and correlation function behavior as lattice models and/or pure fluids, is unanswered. This question is more difficult to answer for mixtures because they have additional thermodynamic variables. For example the "quality" which disappears at the critical point may be thought of as being either a mass density difference or a composition difference between coexisting phases. In principle, if the critical point is approached closely enough, either of these variables (or certain others) could be used to answer the question of universality. Questions analogous to those above may be asked about weak anomalies and transport properties in fluid mixtures. The role of gravity as an experimental limitation to answering these questions is much less clear in the case of mixtures than in the case of pure fluids. This will be discussed briefly below.

2. Opportunities Provided by a low-g Environment.

2.1 Introduction

In this section we will discuss in detail the manner in which gravity affects phase transition and critical phenomena experiments in fluids. We will see that gravity limits the closeness with which the critical point may be approached in all earthbound experiments. Thus a low-g environment will provide an opportunity for conducting experiments closer to the critical point than is possible on earth.

Measurements of the equilibrium properties of pure fluids near the critical point can in principle encounter two distinct kinds of limitations because of the earth's gravitational field. One kind of limitation is essentially a technical one. All experiments measure average properties over some finite height. Since the variation of fluid properties with height becomes increasingly large as the critical point is approached, this averaging causes increasing errors as the critical point is approached. In practical cases an important averaging error occurs even for optical measurements (which at first thought might be expected to average over a height of a wavelength of light ~0.5 μm). The size of this "averaging error" depends both upon the property measured and the technique used to measure it. We will consider representative cases below. We will find that for nearly all experiments the closeness of approach to the critical point is limited by averaging errors. These errors may prevent the answering of many of the questions we raised in the last section.

A second kind of limitation to accuracy in the measurement of equilibrium properties of pure fluids which is imposed by the presence of the earth's gravitational field is an unavoidable or "intrinsic" limitation. Relatively

12

simple considerations show that close enough to the critical point the correlation length (or the size of the density fluctuations) for the fluid is limited in the earth's gravity field much as it would be limited if the fluid were placed in a small container. This means that the properties of the fluid itself are altered by the gravitational field. No improvements in experimental technique will enable earthbound experiments to overcome this limitation. To date there are no experiments which are limited by this phenomenon, but it appears that this limit will be approached in the near future.

Gravity enters into the study of the dynamics of phase changes in pure fluids and most fluid mixtures by causing relative motion of the two phases which are almost invariably of different densities. Thus in a 1-g environment a bubble or droplet will rapidly travel to the top or bottom of a macroscopic sample after it has grown to a size of the order of 10 μm. There are a variety of "levitation" techniques for studying droplet and bubble growth which circumvent sedimentation. Unfortunately, none have been demonstrated as being appropriate for studies of pure fluids near critical points where precise control of temperature and pressure are also required.

If the study of binary liquid mixtures were conducted at equilibrium near their critical (consolute) points, "averaging errors" similar to those which occur in pure fluids, would appear. In practice, most binary mixture studies have been conducted at constant temperature but not in diffusive equilibrium so that a different kind of error is present. The diffusion constant tends towards zero at the critical point and diffusive equilibrium may take days or weeks in samples a 1 cm high moderately close to the critical point. It has recently been shown that the "pressure diffusion coefficient" diverges at the consolute point of binary liquid mixtures (Greer et al., 1975; Giglio and

Vendramini, 1975). This divergence indicates "averaging" errors of a different kind may be encountered in liquid mixtures.

We will now discuss these experimental limitations more quantitatively and in more detail.

2.2 Averaging Errors in "Bulk" Experiments.

As a first and most simple illustration of averaging errors we now consider a hypothetical experiment to measure the density of a pure fluid as a function of height exactly at the critical temperature. Such a measurement together with the thermodynamic relation for the gravitation contribution to the chemical potential,

$$d\mu = - mg\ dz \tag{2.2.1}$$

(where g is the acceleration due to gravity, m is the molecular mass, z is the height coordinate increasing upward, and μ is the chemical potential per particle) would make it possible to test the predictions of many model equations of state.

These model equations of state all predict (see appendix A) a critical isotherm of the form

$$\mu - \mu_c = \frac{P_c\ D}{\rho_c} \left| \frac{\rho - \rho_c}{\rho_c} \right|^\delta \ \ \text{Sign}\ (\rho - \rho_c) \tag{2.2.2}$$

(Here μ, P and ρ are the values of the chemical potential, pressure, and number density respectively, and the subscript c indicates the critical value; D is a numerical factor of order unity which varies from fluid to fluid and δ is a "critical exponent" which will be the same for all fluids if universality holds for fluids in the critical region.) Fig. 2.1 shows the outcome of an ideal experiment of this kind with xenon. This figure was constructed using the numerical values for the parameters listed in appendix D. Note that the density can change by more
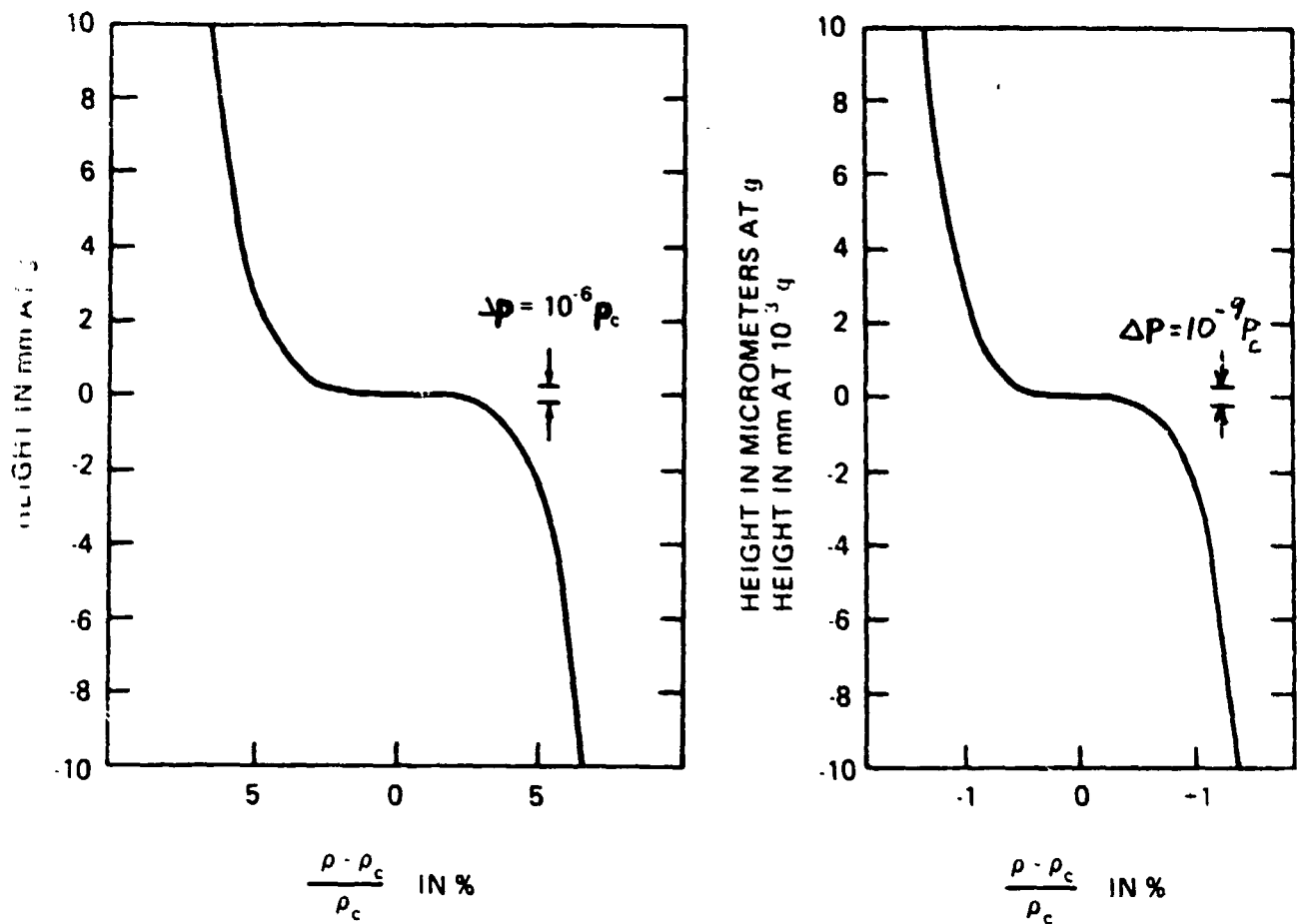
15

Fig. 2.1.   The variation of the reduced density of xenon with height at the
critical temperature.   The calculated curve is displayed on two different scales.
Note that near the critical density, a pressure change of 10^{-6} P_c will cause the
density to change 5% and a pressure change of 10^{-9} P_c will cause the density to
change 1%.

than 5% as a result of a pressure change, ΔP, which is only one one-millionth of the critical pressure. At equilibrium this pressure change occurs (at normal earth gravity, g_o) with a height change from 0.25 mm below the meniscus to 0.25 mm above the meniscus. We have chosen xenon for this numerical illustration (and others in this report) because it is one of the few fluids for which relatively complete data exist in the critical region. It is inert, available in high purity and has a critical temperature near room temperature. (CO_2 and SF_6 are other well studied fluids which are likely candidates for low-g experiments.)

One practical instrument for the measurement of fluid densities in thermal equilibrium at g_o is a float densimeter (Greer et al., 1974). In this instrument the bouyant force on a float of known density is balanced with a spring or magnetic restoring force. The deflection of the spring or the current in the electromagnet is then a measure of $\bar{\rho}$, the difference between the average float density and the average of the fluid density over the float's height. Quantitatively,

$$\bar{\rho} = \frac{\int \rho_{fluid}(z)\ \sigma(z)\ dz}{\int \sigma(z)\ dz} \qquad (2.2.3)$$

where $\sigma(z)$ is the cross sectional area of the float as a function of height. The outcome of a hypothetical experiment with a 1 mm high cylindrical float is shown in Fig. 2.2 (left). The average density $\bar{\rho}$ (points in Fig. 2) differs substantially from the local density at the average height, $\bar{z}$, of the float as soon as any portion of the float overlaps the meniscus. An alternative

17

presentation of the "data" is of interest. We may think of this experiment as one which measures an average "susceptibility", χ_T, of the fluid. This susceptibility is thermodynamically related to the isothermal compressibility and plays a role in the study of fluids which is analogous to the role of the magnetic susceptibility near a magnetic critical point. By definition,

$$\chi_T \equiv \rho^2 \, K_T = \rho^2 \, \left(\frac{-1}{V}\right) \, \left(\frac{\partial V}{\partial P}\right)_T = \left(\frac{\partial \rho}{\partial \mu}\right)_T \qquad (2.2.4)$$

In Fig. 2.2. (right) we compare $\chi_T(z)$ with the average value of χ computed from our hypothetical experimental data by

$$\chi_{exp} = \frac{1}{mg} \left(\frac{\partial \bar{\rho}}{\partial z}\right)_T . \qquad (2.2.5)$$

It is interesting to note that the experiment which measures density by averaging over a finite height is analogous to a spectroscopy experiment with a finite resolution. According to Fig. 2.2, the density experiment has only a limited ability to "resolve" the diverging susceptibility. Details smaller than the resolution are blurred. Yet, some information may be recovered on a scale smaller than the resolution if theoretical guidance is available. For example, if the shape and relative spacings of the spectral lines present in a spectral peak are known accurately in a⁴·ance, their absolute spacing may be determined to much greater accuracy than they can be resolved by the instrument. Similarly, if Eq. (2.2.2) were known to describe the density profile and if techniques were of sufficient quality, accurate measurements of δ, D, and

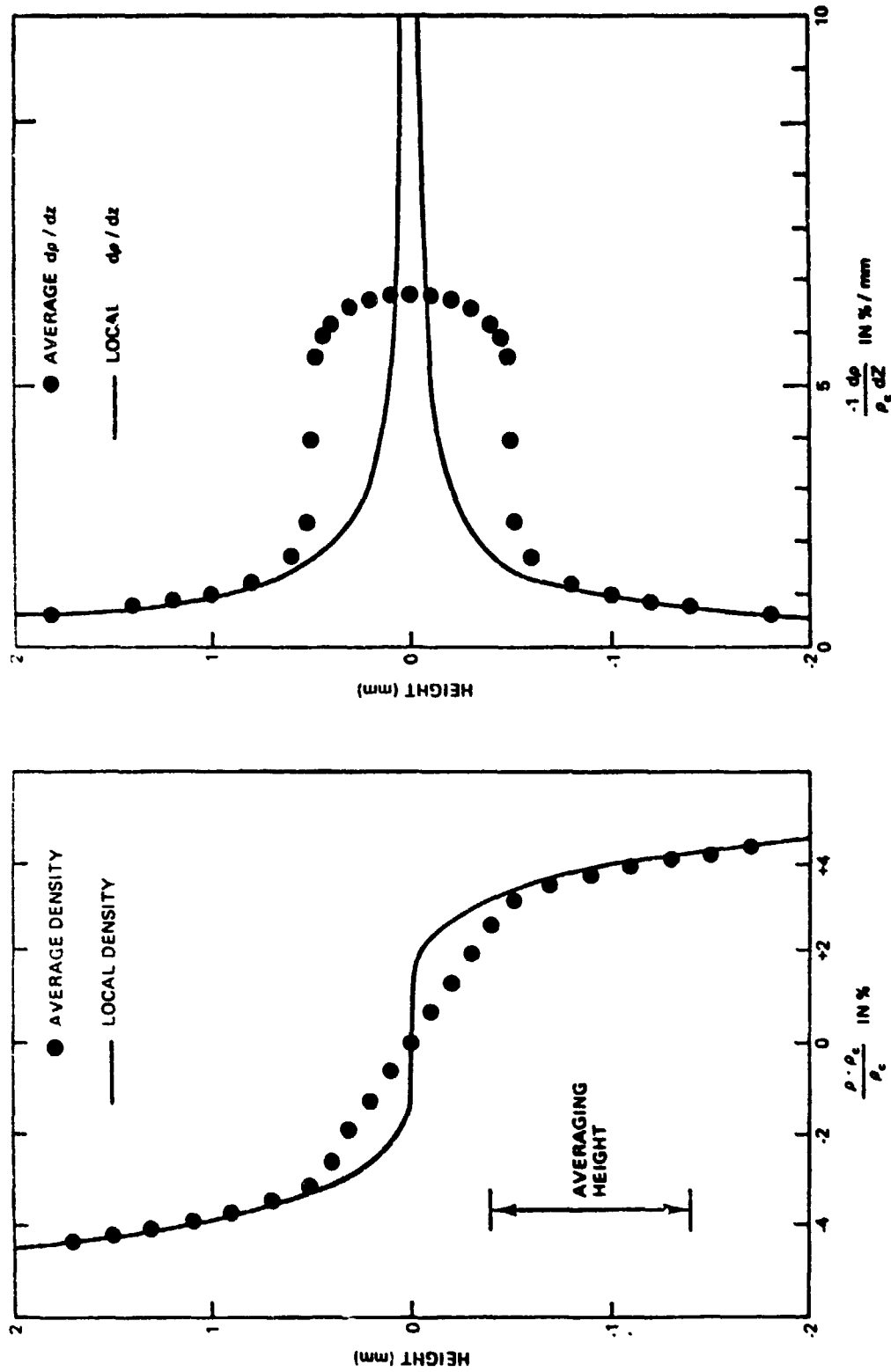Fig. 2.2. Left: The actual reduced density as a function of height (curve) and the reduced density when averaged over 1 mm as a function of the average height (dots). Right: The derivative of the reduced density with respect to height (curve) as a function of height and the derivative of the averaged density with respect to height as a function of height. Both figures are for xenon in the earth's gravitational field.

ρ_c could be obtained with a float of, say, 1 mm height. Unfortunately, the

right hand side of Eq. (2.2.2) is only the first term in an expansion about

the critical density. The higher order corrections to Eq. (2.2.2) are not

known with certainty; thus, the interpretation of data of finite height

resolution becomes subject to the uncertainties arising from different choices

of correction terms. It is at this point that gravitational averaging makes

experimental tests of universality difficult.

A wide variety of realistic experiments have encountered the same density

resolution problems we have illustrated here with the hypothetical density

measuring experiment described above. For example Hohenberg and Barmatz [1972]

have analyzed in detail the effects of gravity averaging upon measurements

of the constant volume specific heat and of the low frequency velocity of sound.

It turns out that both experiments are strongly affected by gravitational

averaging at the critical temperature when the meniscus is within the

experimental cell (see Fig. 2.3). The shortest suitable calorimeters

constructed to date are about 1 mm high and the shortest low frequency

velocity of sound resonator is under 4 mm high, so that both of these

experiments will not resolve the density dependence of the quantity measured

within about 4% of the critical density at normal earth gravity.

The density resolution limit ρ_L scales with sample height, h, and gravity

according to the relation

$$\left|\frac{\rho_L - \rho_c}{\rho_c}\right| = \left(\frac{mg\ h\ \rho_c}{D\ P_c}\right)^{1/\delta} = \left(\frac{h}{DH_o}\ \frac{g}{g_o}\right)^{1/\delta} \qquad (2.2.6)$$

The scale factor for the density profile at the critical temperature, $D\ P_c/(\rho_c\ m\ g_o)$,

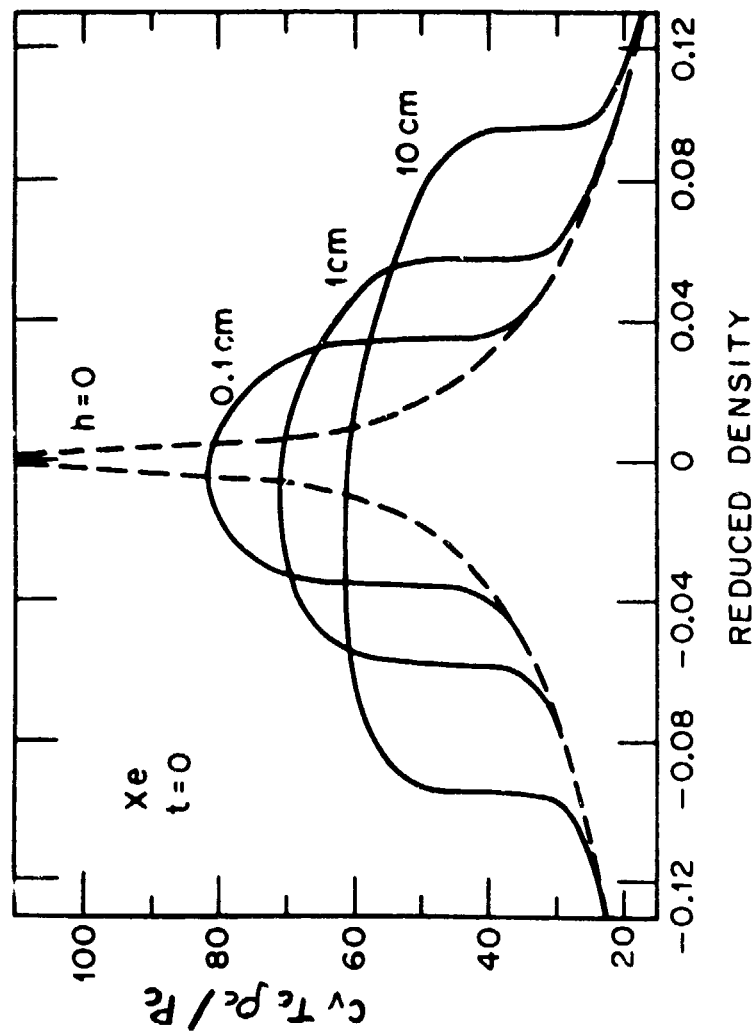varies among 17 fluids (Appendix D) from 910 m in He^3 to 10,400 m in H_2. For

Fig. 2.3. Average specific heat per unit mass C_V vs reduced density $(\rho - \rho_c)/\rho_c$. In order to obtain C_V in J/mole K multiply the ordinate by 2.4. This figure is adapted from P.C. Hohenberg and M. Barmatz, Phys. Rev. $\underline{A6}$, 289 (1972).

xenon, it is 1310 m, a fairly low value among those fluids which are likely

candidates for low g experiments. Because the exponent δ is between 4 and 5

it is clear that a substantial reduction in gh is required to improve density

resolution at the critical temperature. Certain optical experiments

(whose limitations we will discuss below) have averaging heights of micrometers

rather than millimeters, thus optical experiments on earth become potentially

competitive with bulk experiments when the latter are carried out in an

environment of 10^{-3} g.

We have illustrated the density resolution limits at the critical tempera-

tures arising from vertical averaging. The actual resolution is limited at

other temperatures as well. The shape of the resolution limited region is

shown in a qualitative fashion in Fig. 2.4. The true form of the region, of

course, depends upon the particular property being measured and upon the

techniques used. It is straightforward to estimate the extent of the gravity

affected region along the temperature axis as we have done for the density

axis. We will do so in a qualitative fashion here. Then we will indicate

how a more precise criterion for averaging errors could be used to define the

gravity affected region precisely. Such a precise criterion is formulated in

Appendix C.3.

A qualitative idea of the gravity excluded region can be obtained by

noting that the scaling equations of state (Appendix A) indicate that

asymptotically close to the critical point all thermodynamic quantities

(which usually are functions of two variables, say temperature and density)

may be expressed in the simple form $r^P f(\theta)$. Here r and θ are parametric variables

which are related to the temperature and density by nonlinear transformations.

Roughly speaking, r is a measure of the distance from the critical point and θ is

a measure of the distance "around" the critical point from the coexistence curve. The
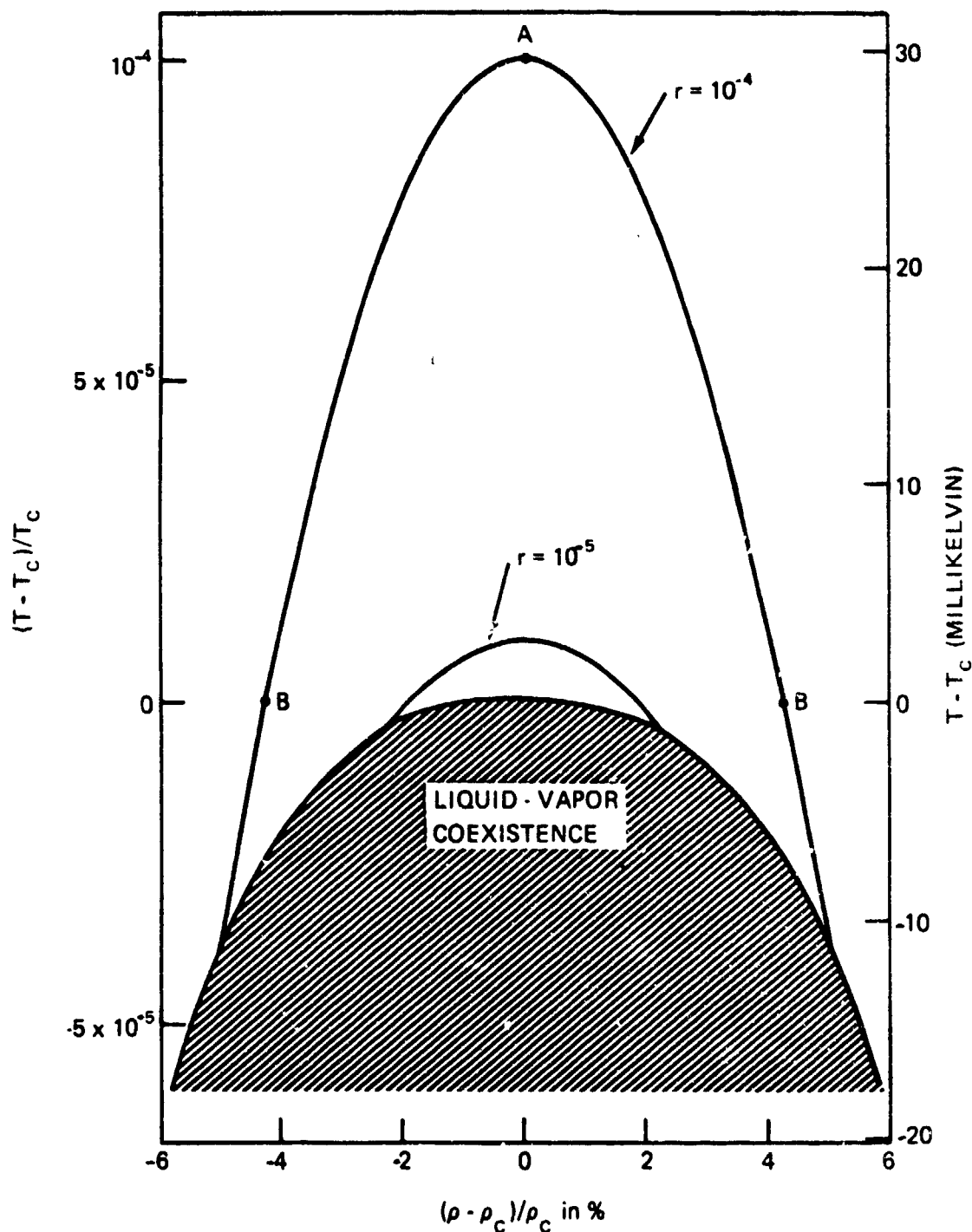
22

Fig. 2.4. Qualitative location of thermodynamic states in the temperature-density plane which are inaccessible to bulk experiments because of gravitational averaging. Averaging errors for a 0.3 cm high sample are substantial beneath the curve marked $r = 10^{-4}$. Averaging errors for a 0.03 cm high sample are substantial beneath the curve $r = 10^{-5}$.

exponent p depends upon the property under consideration, and $f(\theta)$ is an analytic function of θ which also depends upon the property under consideration. In those cases (including the important quantities C_v, K_T and χ_T) where $p < 0$ and where $f(\theta)$ is not a very strong function of θ, the r dependence of the properties becomes dominant near T_c. It follows that divergent quantities will assume approximately the same value along a curve of constant r and such curves have been sketched in Fig. 2.4. It is also true that the gravity excluded region for many experiments is also approximated ! curve of constant r. We have already estimated the gravity limit fo. rements of χ_T and C_v in a sample at the critical temperature, thus locating point B on Fig. 2.4. To find the maximum temperature on the same contour of constant r (point A on Fig. 2.4) we note that in one model equation of state a contour of constant r is identical with a contour of constant χ_T (Appendix A, Eq. A.13). Thus in this model χ_T has identical values at B and A. (In other realistic models the value of χ_T will be nearly the same at B as at A). Now the power law expression for χ_T on the line $\Delta\rho^* = 0$ is

$$\chi_T = \rho_c^2 \ \frac{\Gamma}{P_c} \ (\frac{T-T_c}{T_c})^{-\gamma} \tag{2.2.7}$$

We equate this expression for χ_T with the expression for χ_T along the critical isotherm obtained by differentiating Eq. (2.2.2)

$$\frac{P_c \chi_T}{\rho_c^2} = \frac{1}{D \ \delta} \ |\frac{\rho_L - \rho_c}{\rho_c}|^{1-\delta} = \frac{1}{D \ \delta} \ \left(\frac{gh}{g_o DH_o}\right)^{\frac{1-\delta}{\delta}}$$

$$= \Gamma(\frac{T - T_c}{T_c})^{-\gamma} \tag{2.2.8}$$

24

Using the values of the constants from the appendices we find that the temperature limit for bulk susceptibility measurements is roughly 0.028 K for a 1 mm high sample of xenon and that this limit scales with gravity and sample height as $(gh/g_oH_o)^{0.65}$. If a contour of constant r is used as a gravity limit criterion other experiments will encounter gravity limits at some value of $(T-T_c)/T_c$ which also scales as $(gh/g_oH_o)^{0.65}$.

From the work of Hohenberg and Barmatz [1972], the constant volume specific heat on a 1 cm high cylindrical sample of xenon begins to deviate from the specific heat of a zero height sample by several percent within 50 millikelvin of the critical temperature; for a 1 mm high sample significant error will occur within 12 mK of T_c. Naturally the exact temperature depends on the criterion of accuracy, but with a fixed criterion of accuracy the temperature of closest permissible approach to T_c will scale as $(gh)^{0.65}$. *Thus a substantial improvement in temperature resolution is possible by doing C_v experiments in a low-g environment.* In particular, the determination of T_c in specific heat experiments would be greatly facilitated in a low g environment.

Instead of approximating the region of severe gravitational averaging by a curve of constant r (as we have just done), a precise calculation could have been done. The calculation would involve the following steps: 1) Identify the quantity to be measured (say Q) and the precision with which the quantity is to be known; frequently the desired precision may be expressed as a small fraction, p, of the quantity Q. 2) Examine the measurement technique to determine over what range of heights it averages (say $0 \leq z \leq h$) and with what function (say w(z)) it weights measurements at each height. 3) Compute the values of p and T for which the inequality

$$\frac{1}{h} \int_o^h w(z) \; Q \; (\rho(z), \; T) \; dz \; - \; Q \; (\rho(h/2), \; T) \; \leq \; p \; Q(\rho(h/2), \; T) \qquad (2.2.9)$$

is satisfied. Here we have assumed that the weighted average of Q which the experiment measures will be assigned to the thermodynamic state ($\rho(h/2)$, T) at the midheight of the experiment. Exactly this calculation is carried out in Appendix C where Q is taken to be the correlation length and w(z) is assumed to be unity. A somewhat more complex calculation is required if Q is a quantity measured by experimentally taking a temperature derivative (such as the constant volume specific heat). This problem is discussed by Hohenberg Barmatz [1972].

We have just completed several illustrations of how gravitational averaging influences the measurement of thermodynamic quantities. It is important to note that most measurements of transport properties will also be subject to limited density and temperature resolutions in the earth's gravity. For example the density dependence of the viscosity or of the thermal conductivity cannot be measured within 4-5% of ρ_c, if the viscosity or conductivity apparatus is 1 mm high at earth-normal gravity. It is also true that the density dependence of the turbidity (or total light scattering intensity) cannot be measured within a few percent of ρ_c if the scattering volume is 1 mm high (Leung and Miller, 1975) because of the vertical averaging that occurs in the scattering volume. On the other hand quite different limitations apply to the measurement of thermodynamic and transport properties by optical techniques with very fine spatial resolution. They are discussed in the subsequent section.

2.3 Limitations on Optical Experiments due to Gravity Induced Refractive Index Gradients.

As a fluid is brought near its critical points, its coefficient of isothermal compressibility diverges and, in a gravitational field, the fluid becomes compressed under its own weight. The density gradients thus produced place strong limitations on the validity of measurements, even with optical probes, very near the critical point. The most serious limitation may be termed a "thick cell effect" and applies to all optical experiments including measurements of the phase, intensity and spectral characteristics of light passed through the fluid. Light which is directed horizontally into an optical cell filled with fluid near the critical point will be deflected downward by the index of refraction gradient (resulting from the density gradient). The angle of deflection is proportional to the thickness of the fluid layer in the cell. This effect is precisely the same one which enables the sun to be seen above the horizon several minutes after it has "set" according to astronomical calculations. As the critical point is approached, the density gradients and the deflections become so large that light "rays" pass through layers of fluid of widely varying density. Then it is no longer possible to relate the intensity, the spectrum, or the phase of the light emergent from the cell to the density or any other local thermodynamic variable. The measurable optical properties of the fluid become complex gravitational averages. In this section we discuss and quantify these limitations for optical experiments using a combination of analytical and numerical techniques.

Consider a sample of a dielectric fluid, in a cell with plane parallel optical windows, with an average density, ρ_o, closely approximating the critical density. When the sample temperature is held constant near T_c, the

27

fluid is compressed under its own weight and an equilibrium density distribution, $\rho(z,T)$, is formed. Since, in a gravitational field, the reduced chemical potential μ is directly proportional to z, the density profile is directly given by the equation of state $\rho(\mu,T)$. Furthermore, if current theory is correct (Appendix A) such profiles are antisymmetric about some density ρ_{cen} (ρ_{cen} is not necessarily the critical density and in general will be a function of the temperature. For this analysis we will assume that $\rho_{cen} = \rho_c$) which occurs at the height where the compressibility has a maximum. The plane at this height, which we call the centrus, will serve as the origin for our vertical coordinate system. In Figure 2.5 we represent such a profile schematically for some supercritical temperature $T > T_c$. (All of our analysis will deal only with the one phase region.) Because the refractive index of the fluid is related to its density by the Lorentz-Lorenz (Lorenz, 1880; Lorentz, 1952; Hocken and Stell, 1973; Larsen et al., 1965) formula, there is a corresponding refractive index profile n(z,t) in the sample. Now we illuminate the optical cell with a monochromatic horizontal (normal to the z axis) plane wave of light, and examine the trajectories of rays through the profile at various heights.

In Fig. 2.6 we illustrate this situation with a simple ray picture. A ray enters the cell horizontally at height z' above the centrus and is refracted downward on a curving trajectory until it emerges at a height z. The output angle of the real ray will be proportional to the average refractive index gradient 'seen' by the ray and its phase shift will be determined by an average over its optical path. Also shown in the same figure are two ideal rays which we call 'thin cell' rays. Both are equivalent to the real ray when the cell is infinitely thin or the gradient so small that $z' \approx z$. They are

28
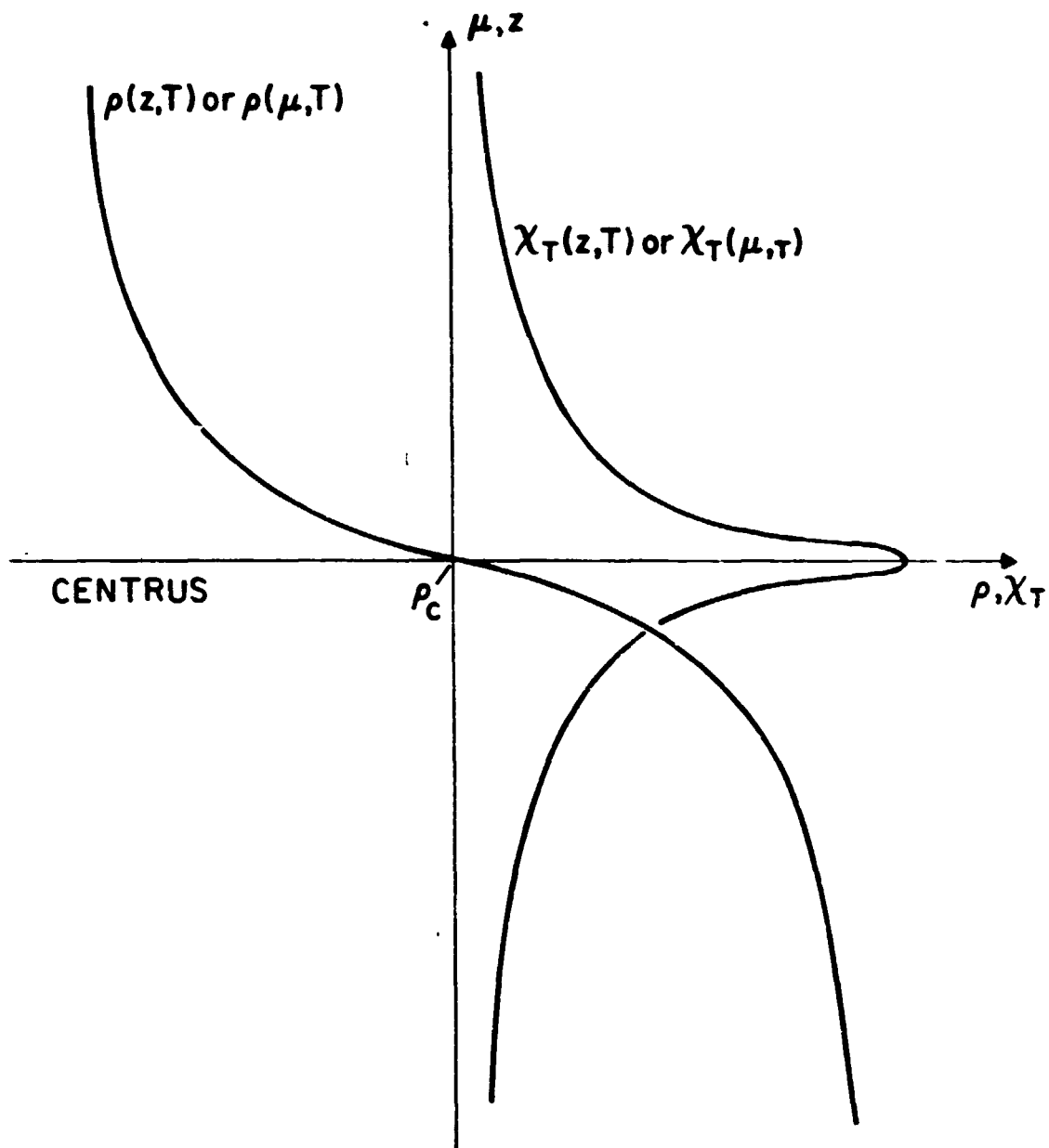
Figure 2.5. Schematic of density and compressibility profiles.
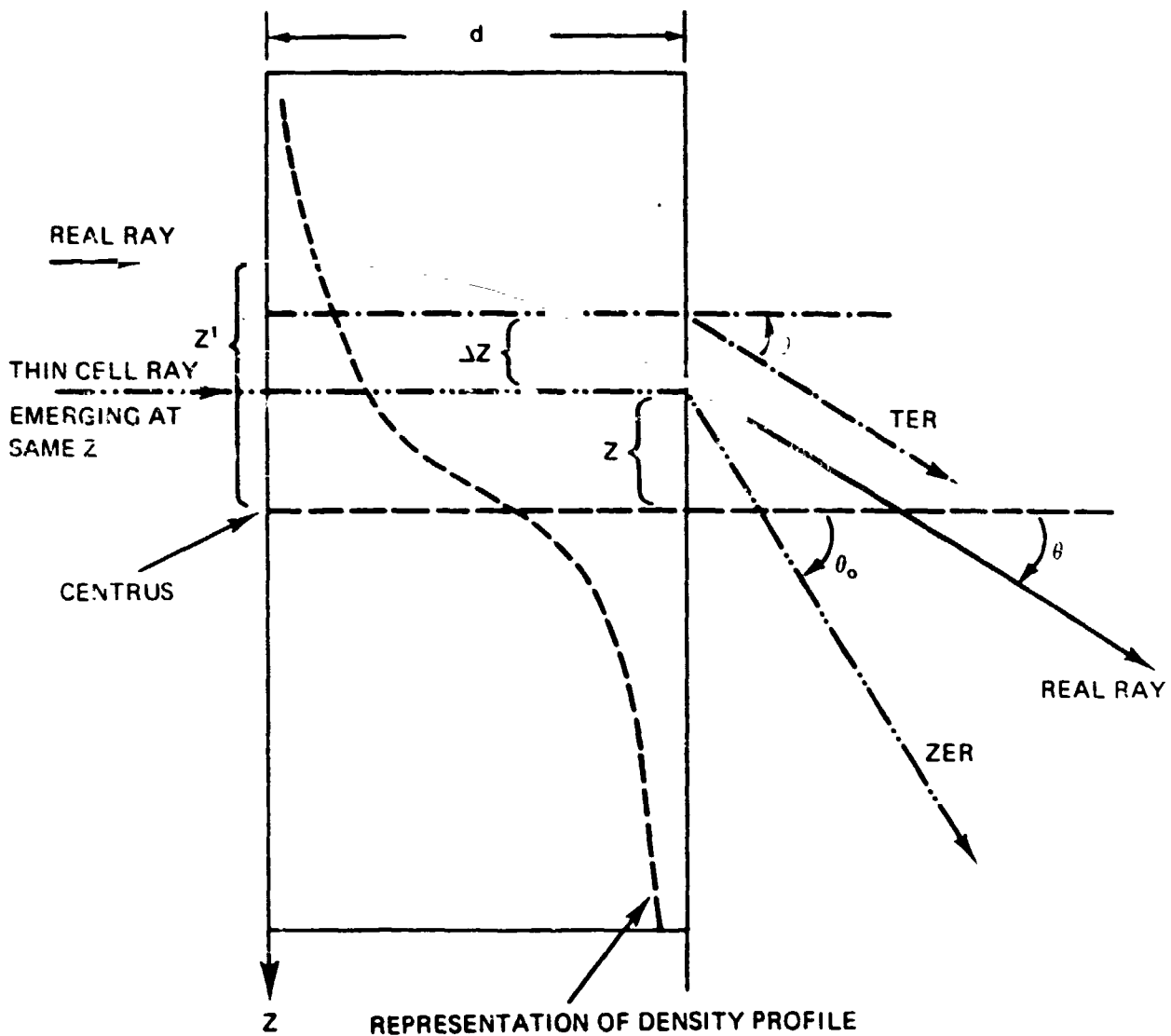
Fig. 2.6. Rays through a density profile. "Real ray" denotes the path
traversed by a light ray incident horizontally upon an optical cell filled
with fluid near the critical point. The other rays are defined as follows: the
angle equivalent ray (TER) is that thin cell ray which is refracted at an angle
equal to the real ray. It traverses the cell horizontally at a height $(z + \Delta z)$
where the local refractive index gradient is equal to the average gradient seen
by the real ray; the height equivalent (ZER) is that thin cell ray which traverses
the cell horizontally at height z.

defined as follows: the "angle equivalent" ray (TER) is the thin cell ray which

is refracted at an angle equal to the real ray; it traverses the cell

horizontally at a height $(z + \Delta z)$ where the local refractive index gradient is

equal to the average gradient seen by the real ray . The "height equivalent" ray

(ZER) is that thin cell ray which traverses the cell horizontally at height z.

These thin cell rays are introduced for comparison purposes since for them

the relation of optical observables to thermodynamic quantities is particularly

simple (Estler et al., 1975). For instance, if we expand the Lorentz-Lorenz

formula, we find to a good approximation that

$$n - n_c = n_1 \left(\frac{\rho - \rho_c}{\rho_c}\right) + \ldots = n_1 \Delta\rho^* + \ldots$$

$$(n_1 \equiv \frac{(n_c^2 - 1)(n_c^2 + 2)}{6\, n_c}).$$

(2.3.1)

Then the index gradient becomes

$$\frac{dn}{dz} = n_1 \frac{d\rho^*}{dz} = \frac{n_1}{H_c}\left(\frac{\partial\rho^*}{\partial\mu^*}\right)_T = \frac{n_1}{H_0}\, \chi_T^*$$

(2.3.2)

where μ^* is the reduced chemical potential, χ_T^* the reduced susceptibility

and $H_0 = P_c/(\rho_c m g)$, the scale height for the fluid being studied. In the thin cell

limit the ray ZER simply comes out at height z with an angle proportional to

χ_T^* at that height, i.e.

$$\chi_T^*(z) = \frac{H\theta(z)}{dn_1}, \text{ for the ZER,} \qquad (2.3.3)$$

where d is the cell thickness.

Fig. 2.7 offers a comparison between angles of rays as a function of z as determined from equation (2.3.3) and angles determined numerically by tracing rays (Born and Wolf, 1975) through the same density profiles. The profiles were generated using the Stony Brook parametric equation of state (Wilcox and Estler, 1971) with parameters obtained from actual profile measurements on xenon (Estler et al., 1975). The parameters used are given in Appendix E. The computation was performed with $\Delta T^* = \frac{T-T_c}{T_c} = 5\times10^{-6}$. The solid line represents the thin cell results for the ZER (Eq. 2.3.3) and terminates in a rounded point at an angle of about .17 radians, that is, off the graph. The dashed line is the result of the ray tracing computation. The crosshatched region contains rays that enter the cell close to the centrus above and below and emerge at approximately the same height but at very different angles; the observer sees a bright band at this height with a darker band above it. In this region the gradient is so large that the rays are simply bent right out of the dark region and into the bright band.

Fig. 2.8 shows the same results for the optical phase as a function of height. Again the solid line is the thin cell result, i.e. neglecting any beam bending effects, (cf. (2.3.3) and the dashed line is the result of ray tracing. The optical phase relative to that at the centrus $(\Delta\phi)$ is simply related to the density in the thin cell approximation:

$$\Delta\phi = - k \, d \, n_1 \, \rho^*(z) \qquad (2.3.4)$$
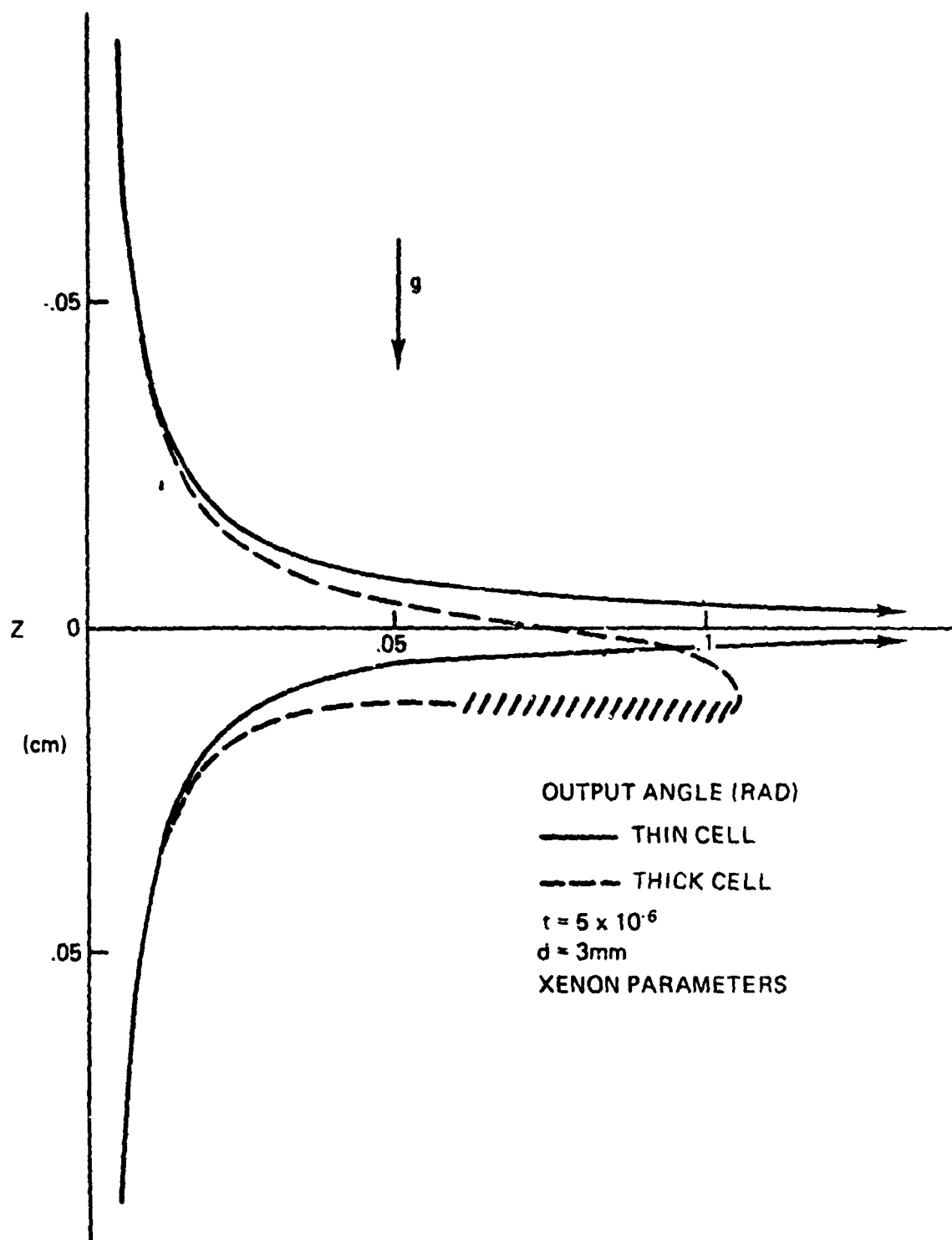
Fig. 2.7.   The angles of emergent rays as a function of height. The solid
line represents the thin cell results for the ZER (eq. 2.3.3) and terminates in
a rounded point at an angle of about .17 radians, that is, off the graph. The
dashed line is the result of the ray tracing computation. The crosshatched
region contains rays that enter the cell close to the centrus above and below
and emerge at approximately the same height but at very different angles.

33
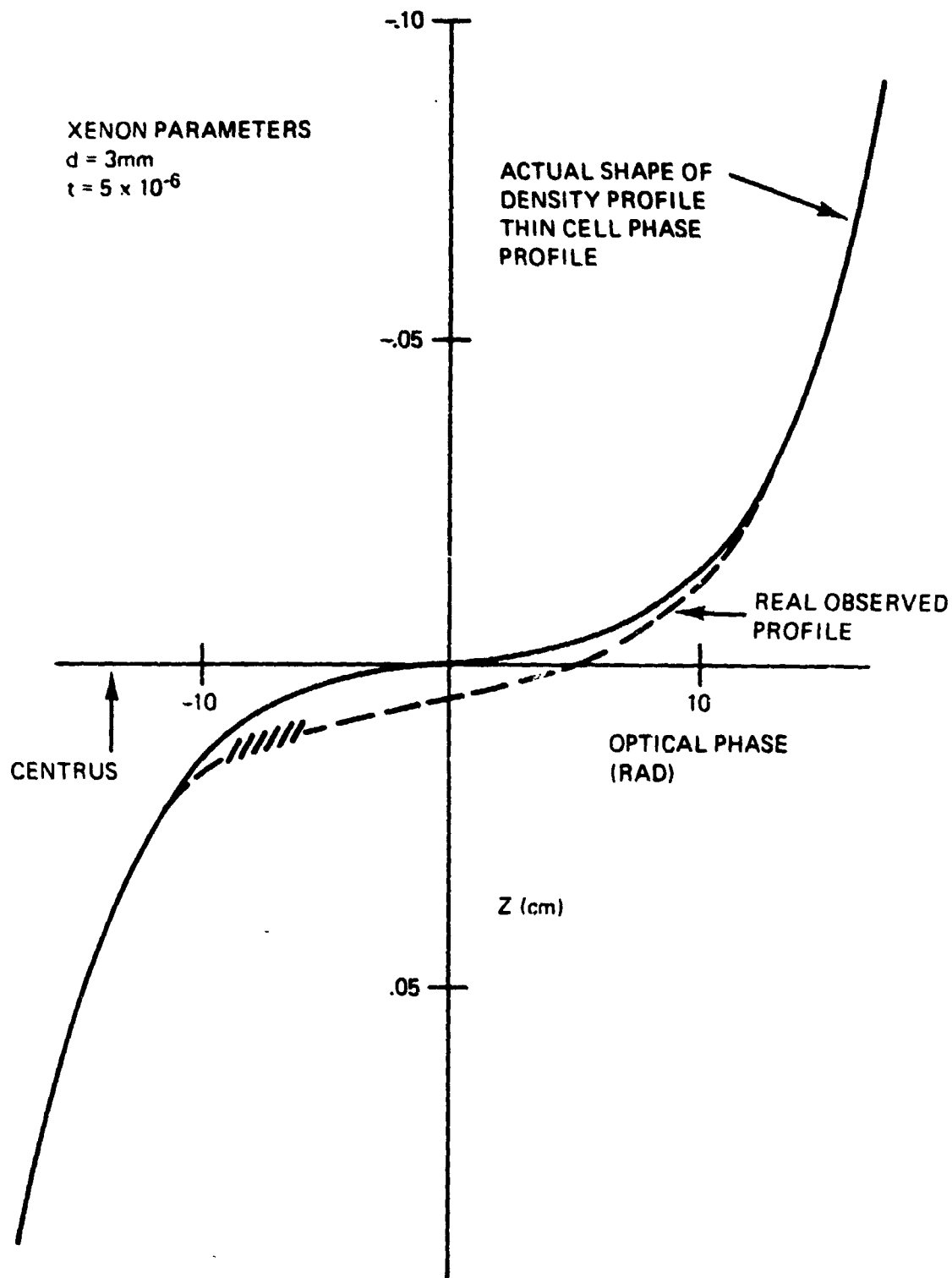
Fig. 2.8. Optical phase as a fur tion of height. The phase profile calculated in the thin cell approximation (solid curve) has the same shape as the density vs height profile. The observed profile is represented by the dashed curve. The crosshatched area corresponds to the crosshatched area in Fig. 2.7.

Hence, the solid curve is, except for sign and units, simply the existing density profile. The dashed line is then the apparent density profile deduced from actual measurements and in fact such "kinked" profiles have been reported in the literature (Lorentzen and Hansen, 1966).

Figures 2.7 and 2.8 offer a good visual picture of what happens to light traversing a fluid near its critical point. They do not, however, offer simple quantitative guidelines as to which regions of the thermodynamic space are inaccessible to the earth bound experimenter. To provide these guidelines we found it convenient to compare the real ray with the angle equivalent ray (TER) rather than to the ZER as in Figs. 2.7 and 2.8.

As our computations progressed we discovered numerically a simple relationship between Δz (the height difference between the TER and the real ray, see Fig. 2.6) and the output angle of the real ray (or TER since they are defined to be the same). We then derived this expression for Δz by solving the ray tracing equations analytically in a medium where dn/dz was a slowly varying function of height. We found that if

$$\frac{dn(z)}{dz} \approx \frac{dn}{dz}\Big|_{z_c} + \frac{d^2 n}{dz^2}\Big|_{z_o} (z - z_o), \qquad (2.3.5)$$

then

$$\Delta z \approx \frac{n_1 d^2}{3 \text{En}_c} \cdot \chi_T^*. \qquad (2.3.6)$$

As long as equation (2.3.6) holds, the real ray carries average fluid

35

information equal to the local information at a height Δz above the height of the real ray's emergence. This equation is valid both above and below the centrus.

We then performed computer experiments to test the domain of validity of (2.3.6) using numerical parameters appropriate for xenon. We found that (2.3.6) breaks down when Δz reaches a certain value nearly independent of the temperature and the fluid studied. The results are plotted in Fig. 2.9 for xenon. In this figure the solid dark line represents the Δz that would be calculated from (2.3.6) using the fluid's maximum compressibility. That is

$$\Delta z_{max} = \frac{n_1 d^2}{3 \, H n_c} \, \chi^*_{T_{max}} = \frac{n_1 d^2}{3 \, H n_c} \, \Gamma \left| \Delta T^* \right|^{-\gamma} . \qquad (2.3.7)$$

The region above and to the right of this curve is nonphysical: no real thermodynamic states exist in this region. The area below this curve and to the left is physical but mostly inaccessible to the earth bound experimenter. On this plot the critical point is at infinite Δz. The dashed line at $\Delta z \approx .002$ cm represents the contour where (2.3.6) becomes incorrect by 1%. Above this line the errors grow very rapidly. The region below this line is experimentally accessible and here the properties of the interference pattern may be simply related to local thermodynamic properties of the fluid. As a simple rule of thumb we find that the observed interference pattern can no longer be simply related to local thermodynamic fluid properties when the reduced compressibility
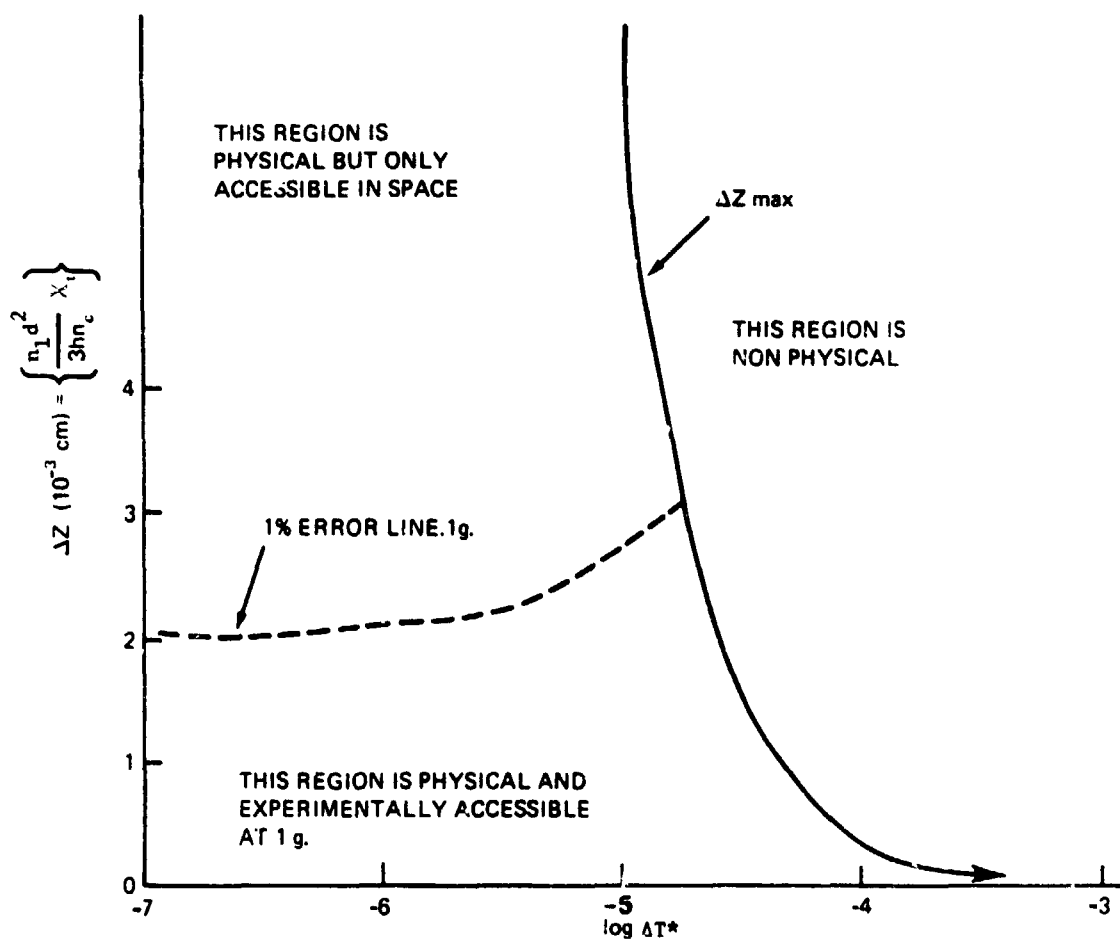
Fig. 2.3.   Thermodynamic states acces 'bl₂ to optical experiments.   The
states with sufficiently small values of the scaled compressibility χ_T are
accessible.   Large valu₂s of χ_T do not occur to the upper right of the solid
curve (i.e. far from the critical point).

becomes larger than

$$x^*_{T_{max}} = (.002 \text{ cm}) \frac{3 H n_c}{n_1 d^2} .$$ (2.3.6)

It is convenient to tabulate some examples for comparison with gravitational limits provided elsewhere in this report. We do so here for xenon

Cell Thickness cm.	$x^*_{T_{max}}$	θ_{max} milliradians	$\Delta\rho^*_{min}$ ($\Delta t^* = 0$)	ΔT^*_{min} ($\Delta\rho^* = 0$)
1.0	2.6×10^3	22	0.0471	1.6×10^{-4}
0.1	2.6×10^5	220	0.0119	3.3×10^{-6}

Thus any optical experiment using a 1 cm thick cell is subject to limitations comparable to a bulk experiment in a 0.1 cm high cell at g_o. An optical experiment in a 0 1 cm thick cell is subject to limitations comparable to a bulk experiment in a 3 μm high cell at g_o or a 3 mm high cell at $10^{-3} g_o$. Optical cells with properties suitable for critical point experiments (Hocken et al., 1975) have been fabricated with a thickness of 3 mm. It seems likely that 1 mm thick cells could be made. The feasibility of making much thinner cells should be examined. One may expect that fluid samples in extremely thin cells would be subject to contamination from the cell walls because of the large surface to volume ratio.

2.4 Light Scattering Measurements and Some Gravity Related Limitations.

Scattering measurements provide a means to measure the space-time dependence of fluctuations. Since much of the fundamental picture of critical fluctuation phenomena deals with the distance scale over which fluctuations are correlated (space) and the time scale over which fluctuations grow and decay (time),scattering spectroscopy continues to be an important tool for studying critical phenomena.

Near the gas-liquid critical point a fluid exhibits large fluctuations in the density. The magnitude of these fluctuations is proportional to the compressibility. The spatial extent of these fluctuations can be characterized by a correlation length ξ. As shown in Appendix C this correlation length is related to the compressibility by

$$\xi = \xi_o \, (\Gamma^{-1} \chi_T^*)^{\frac{1}{2-\eta}} \qquad (2.4.1)$$

where χ_T^* is the dimensionless symmetrized compressibility defined in A.2. The constants ξ_o and Γ are the amplitudes in the power laws (C.4) and (A.4c) for the correlation length and compressibility along the critical isochore. The constant ξ_o is a microscopic distance of the order of the range of the intermolecular forces.

The spectral intensity as a function of scattering angle and frequency is proportional to the spatial and temporal Fourier transform of the time dependent correlation function of the order parameter. In a one component fluid the integrated intensity of the scattering is proportional to the static structure factor

39

$$S(k) = \int d\vec{R} \, e^{ikR} G(R) \qquad (2.4.2)$$

where the correlation function $G(R)$ is defined in Appendix C. The wave number k is related to the scattering angle θ by

$$k = 2 \, k_o \sin \frac{\theta}{2} \qquad (2.4.3)$$

where k_o is the wave number of the incident radiation.

In principle $S(k)$ is a function of temperature ΔT^*, density $\Delta \rho^*$ and wave number k. However, according to the scaling hypothesis the structure factor near the critical point can be written in the form (Fisher, 1967)

$$S(k) = \xi^{2-\eta} \, \psi(k\xi) \qquad (2.4.4)$$

where ξ is the correlation length. This reduction of the description is valid for any thermodynamic path in the $\Delta T^* - \Delta \rho^*$ plane of constant scaling variable, i.e. ΔT^* proportional to $|\Delta \rho^*|^{1/\beta}$. Here we shall consider specifically the properties of scattered light at the critical isochore $\Delta \rho^* = 0$.

The scaled function $\psi(k\xi)$ is known theoretically (Tracy and McCoy, 1975) for the 2 dimensional Ising model for all values of $k\xi$. However, the mathematical form of this function for fluids is not known except for the fact that it must approach a constant in the limit $k\xi \to 0$ and that it must vary as $(k\xi)^{-2+\eta}$ for $k\xi \to \infty$.

It has turned out to be very difficult to determine a definitive value for the exponent η. A precise knowledge of this exponent has a direct bearing

40

on the question of universality of the pair-correlation function.

In order to determine this experimental η with any accuracy, measurements are needed for $k\xi$ sufficiently large so that the function $\psi(k\xi)$ can be approximated by its asymptotic behavior (Tracy and McCoy, 1975). Due to limitations caused by multiple scattering and the gravity induced density gradients, it has been impossible to satisfy this condition for earth bound light scattering experiments. It has been possible to reach sufficiently large values of k with neutron scattering (Warkulwiz et al., 1975); however, here one has difficulties in satisfying the condition that k^{-1} must be large compared to the range of the intermolecular forces.

Of the several available scattering techniques (light, X-rays and neutron scattering), optical light scattering using laser sources seems to be most feasible one for space experiments. It is the only scattering technique with sufficient spectral resolution to examine the narrow spectrum of the fluctuations, can be done with easily portable sources (lasers), requires no radiation shielding, and uses windows compatible with other optical records desired of the sample behavior. The principle drawback to light scattering mea: .rements is multiple scattering: the extinct'on of the beam gives a severe lower limit on the ΔT^* which can be reached. Numerical estimates for this limit are presented later in this section.

Using optical beating techniques, one can measure the spectrum of the quasi-elastic Rayleigh line (Cummins and Swinney, 1970). The width of this line is related to the diffusive decay constant of the fluctuation of the order parameter. A survey of the current status of the experimental work on Rayleigh scattering near the critical point of fluids has been given by Swinney and Henry [1973].

41

In interpretating such experiments one usually introduces the following assumptions. First it is assumed that fluctuations still decay exponentially in time so that the dynamic structure factor has the form

$$S(k,\omega) = S(k) \; \frac{2\Gamma_s}{\Gamma_s^2 + \omega^2} \tag{2.4.5}$$

where Γ_s is the decay rate of the entropy fluctuations. (Swinney and Henry, 1973). Secondly, one uses the assumption of dynamical scaling to write the decay rate Γ_s in the scaled form

$$\Gamma_s = \xi^{-3} \; \psi_\Gamma \; (k\xi) \tag{2.4.6}$$

It should be pointed out that these assumptions are not valid rigorously, and that one expects to see deviations if the critical point is approached sufficiently closely. Theories for the scaled function $\psi_\Gamma(k\xi)$ have been developed by Kawasaki and coworkers and by Ferrel and Perl; for a survey of the literature the reader is referred to the article by Swinney and Henry [1973]. The various theories differ in their conclusions, but it has been impossible to discriminate between the theories on the basis of earthbound experiments.

For light scattering measurements we need to consider the limitations on the attainable experimental precision due to gradients in the density $\Delta\rho^*$, turbidity of the sample, and gradients in the correlation length ξ. Our purpose here is to estimate how much the accessible range in ΔT^* and $\Delta\rho^*$ can be extended by conducting light scattering experiments at reduced g.

42

We first consider the variation in density. In a light scattering experiment close to T_c one can consider using a weakly focused beam with a diameter of ≥ 100 μm. Stronger focusing would require much lower power levels to avoid local heating particularly at window surfaces. Thus there exists a practical height or spatial scale limit for critical point light scattering measurements of about 100 μm.

The resolution of light scattering experiments has been exploited in earth-bound experiments by moving the beam as a function of height, thus obtaining local equilibrium isothermal scattering intensities (White and Maccabee, 1975) and spectra (Swinney and Henry, 1973; and Kim, et al., 1974). In order for the density change over a height to be within a precision p of the average density in that region for a sample in a gravitation acceleration $g^*(g^* = g/g_o)$, we require

$$\frac{d}{dz} \Delta\rho^* \; h \leq p \tag{2.4.7}$$

Using the restricted cubic model and Eqs. A.13 and B.7 of the Appendices, we find

$$r \geq (\frac{hg^*}{p} \; \frac{k_2}{H_o a_2})^{\frac{1}{\gamma}} \tag{2.4.8}$$

)

43

For xenon, using parameters of Appendix D, we find

$$r \geq 6.2 \times 10^{-4} \left(\frac{h g^{*}}{p}\right)^{.84} \qquad (2.4.9)$$

with h in meters. Thus this density limit is a contour of constant r in the (ΔT^{*}, $\Delta \rho^{*}$) plane as discussed in Section 2.2. The following table gives examples of the lower bounds to r and corresponding $\Delta T^{*} = r$ (with $\Delta \rho^{*} = 0$) and $\Delta \rho^{*}$ (with $\Delta T^{*} = 0$), for p = .01 $\equiv$ 1%, h = 10^{-4} m $\equiv$ 100μm corresponding to precision scattering experiments on earth (1g), worst case Shuttle accelerations (10^{-3}g) and best case Shuttle accelerations (10^{-6}g).

Table 2.4.1

$g^{*} = g/g_{o}$	$r = \Delta T^{*}$ ($\Delta \rho^{*} = 0$)	$\Delta \rho^{*}$ ($\Delta T^{*} = 0$)
1	1.3×10^{-5}	1.9×10^{-2}
10^{-3}	3.9×10^{-8}	2.4×10^{-3}
10^{-6}	1.2×10^{-10}	3.0×10^{-4}

Next we examine the effect of the strong (critical opalescense) scattering of light in the sample. The density fluctuation scattering cross section per unit volume per stearadian of a fluid is given by

$$\frac{d(1/V)}{dr} = \pi^{2} \frac{\sin^{2}\phi}{\lambda^{4}} (\rho \frac{\partial \epsilon}{\partial \rho})^{2} k_{B} T K_{T} \qquad (2.4.10)$$

44

where λ is the wavelength of the incident beam (in vacuum), ϵ is the optical dielectric constant at λ and K_T is the isothermal compressibility and ϕ the angle between the incident light polarization and the scattered wavevector. Near the critical point K_T has a strong temperature dependence leading to the result that the scattering intensity diverges like K_T. For $k = 2\pi/\lambda << \xi^{-1}$, this dipole cross section can be readily integrated over all angles to give the scattering attenuation coefficient called the turbidity, τ

$$\tau = \frac{8\pi^3}{3} \frac{1}{\lambda^4} (\rho\frac{\partial\epsilon}{\partial\rho})^2 k_B T K_T \qquad (2.4.11)$$

For the present estimates we have neglected the angle dependence of the scattering due to the correlation length ξ (see Puglielli and Ford, 1970 and Cannell, 1975).

Like the cross section, the turbidity follows the temperature dependence of K_T. Using the cubic model (Appendix A.3) we can write for K_T

$$K_T = (\frac{k_2^2 \rho_c^2}{a_2 c}) \frac{r^{-\gamma}}{\rho^2} \qquad (2.4.12)$$

Since close to the critical point $\rho \stackrel{\sim}{=} \rho_c$, we find that τ is proportional to $r^{-\gamma}$.

In light scattering studies the intensity corrections due to turbidity become severe for a path length ℓ such that $\tau\ell \geq 1$. At approximately the same $\tau\ell$ limit the corrections due to multiply scattered light reaching the detector become severe. Thus we see that scattering experiments are limited to studying the samples for $\Delta T^* - \Delta\rho^*$ such that $\tau < \ell^{-1}$.

We have evaluated the turbidity and the resulting limitations for the case of xenon using the parameters of Appendix E at $\lambda = 6328\text{Å}$ (He-Ne laser), and

45

and approximating $(\rho\frac{\partial\epsilon}{\partial\rho}) \approx (\epsilon_c - 1)$. We find

$$\tau = 2.51 \times 10^{-3} \; r^{-1.19} \; (m^{-1}). \qquad (2.4.13)$$

For an optical path ℓ (m) we conclude that r must satisfy

$$r \geq 6.53 \times 10^{-3} \; \ell^{.84}. \qquad (2.4.14)$$

Typical optical cells at present have $\ell = 10^{-2}$ m (1 cm). More specialized cells have been made with $\ell = 10^{-3}$ m (1 mm). It may be feasible to work with $\ell = 10^{-4}$ (100μm). With such a thin cell one must carefully discriminate against scattering from the inner cell walls. These distances have been used to calculate the lower bounds of r and corresponding ΔT^* and $\Delta\rho^*$. For xenon and $\lambda = 6328\text{Å}$ we find:

Table 2.4.2

Turbidity approach bounds at $\lambda = 6328\text{Å}$ in Xenon

ℓ(m)	$r = \Delta T^*$ $(\Delta\rho = 0)$	$\Delta\rho^*$ $(\Delta T^* = 0)$
10^{-2}	1.4×10^{-4}	4.4×10^{-2}
10^{-3}	2.0×10^{-5}	2.2×10^{-2}
10^{-4}	2.8×10^{-6}	$1.1 \times 10^{-2)}$

46

Comparison of Tables 2.4.1 and 2.4.2 shows that at 1g, a 1 mm optical path cell of xenon has both the density profile and turbidity limit of about $r = 1.\times10^{-5}$. This limit corresponds to $\Delta T \approx 3$ mK. In order to take advantage of decreased density gradients at 10^{-3}g one would need a cell with optical path less than 100µm $\equiv 10^{-4}$m. The ability to fabricate such a cell has not been demonstrated. Thus we see that turbidity and multiple scattering place a severe bound to scattering experiments closer to the critical point. On earth at 1g this has not been as severe because the sample density gradients have caused most of the sample to be off the critical density giving reduced scattering and turbidity. In a low g environment one expects to see the sample uniformly opalescent and becoming quite opaque to visible wavelengths as the critical point is approached. The fact that the sample is uniformly opalescent at low g should make the analysis of the influence of multiple scattering much more manageable. The new theoretical work on multiple scattering (Reith and Swinney, 1975; Bray and Chang, 1975) will be helpful in the analysis of low g scattering data.

It is clear that for studies close to the critical point one needs to reduce the observed turbidity. This can be done with the choice of λ or choice of fluid with a small defractive index. Since the turbidity varies as λ^{-4}, the turbidity at a given ΔT^* could be greatly decreased by using longer wavelengths. Small continuous He - Ne lasers exist at 1.152µm and 3.391µm. Photomultipliers still work at 1µm so this choice would be favored for spectral measurements and would decrease the tubidity by 10.9x and the r bound by 7.5x. At 3µm photoconductive detectors would be required. The quantum efficiency may be so low that beating spectra of the critical fluctuations may not be possible. Also the choise of window materials becomes more restricted. The following table shows the turbidity bounds of ΔT^*, $\Delta\rho^*$ in xenon: for electromagnetic radiation with a wavelength of 3µm.

47

Table 2.4.3

Turbidity approach bounds at $\lambda = 3.391\mu$ in xenon

$\ell(m)$	$\tau = \Delta T^*$ $(\Delta\rho^* = 0)$	$\Delta\rho^*$ $(\Delta T^* = 0)$
10^{-2}	4.8×10^{-7}	6.0×10^{-3}
10^{-3}	7.0×10^{-8}	3.0×10^{-3}
10^{-4}	1.0×10^{-8}	1.5×10^{-3}

Table 2.4.3 indicates that at 3.391µm we could exploit the 10^{-3} g environment with 100µm path cells, over a new range of $\Delta T^* = 10^{-5}$ to 10^{-8} and $\Delta\rho^* = 2 \times 10^{-2}$ to 2×10^{-3}. With 6328Å we could only go in to $\Delta T^* = 10^{-6}$.

Alternatively we can consider going to a fluid with lower dielectric constant, $\varepsilon = n^2$. The best choice (lowest ε) would be the rare isotope of helium, He^3. Here $n_{6328} = \approx 1.0108$ in the fluid near T_c. (We have taken n_c for He^4 from the data of Edwards and Woodbury [1963] and scaled it for He^3 using the Clausius- Mosotti relation with the critical densities from Appendix D). Thus at 6328Å we expect $\tau_{He}/\tau_{Xe} = (\varepsilon_{He}-1)^2/(\varepsilon_{Xe}-1)^2 = 1/153$. One could further reduce τ_{He} by moving out to 1µm or 3µm. Thus, the use of helium would help overcome the increase in turbidity encountered upon approaching the critical point at the cost of doing experiments at cryogenic temperatures (3.3 K).

The angle dependence of scattering intensity and linewidth closer to the critical point are of interest because of questions concerning the theory of the fluctuations in the non-hydrodynamic region. The angle dependence of intensity is written in scaled form in (2.4.4). At a fixed ΔT^*, $\Delta\rho^*$ the angle dependence arises from the function $\psi(x)$ with $x = k\xi$ and $k = 2 k_o \sin \theta/2$. Similarly, the scattering angle dependence of the decay rate Γ_s is given

by (2.4.6) and comes from x in the function $\psi_\Gamma(x)$. If the measurements are to be used to determine ξ or to test the form of $\psi(x)$ or $\psi_\Gamma(x)$ it is essential that we know x precisely. If ξ varies over the sample or specifically over the diameter of the probing beam in the sample due to gravity gradients then x is correspondingly poorly defined. Assuming for the moment that k is well defined through suitable collimation of the incident and scattered beams, the measurement precision of $x = k\xi$ will be limited by the uniformity of ξ.

We ask that ξ be constant to a precision p over a height $h = 10^{-4}m \equiv 100\mu m$ or

$$\left(\frac{d\xi}{dz}\right)_T h \leq p \, \xi \tag{2.4.15}$$

Using the results of Appendix C for $\left(\frac{d\xi}{dz}\right)_T$ one can use (2.4.15) to give $r(\theta)$ and then transfer to ΔT^*, $\Delta\rho^*$. We have done this for xenon with $p = 0.1$, $h = 10^{-4}m$ giving the lower bound ΔT^*, $\Delta\rho^*$ contours shown in Fig. 2.10 for $g^* = 1$, 10^{-3} and 10^{-6}. Comparing the figure to Table 2.4.3 shows that even if the turbidity limit is lowered by changing to 3μm wavelengths we will begin to be limited for $g^* = 10^{-3}$ by the correlation length gradient.

There is a further effect of turbidity in determining x. This occurs because k is well defined only for non-attenuated incident and scattered waves. Attenuated waves give a spread to k. To have k defined to 1% we need $k > 10\tau$. Since $k \simeq x/\xi$, we require
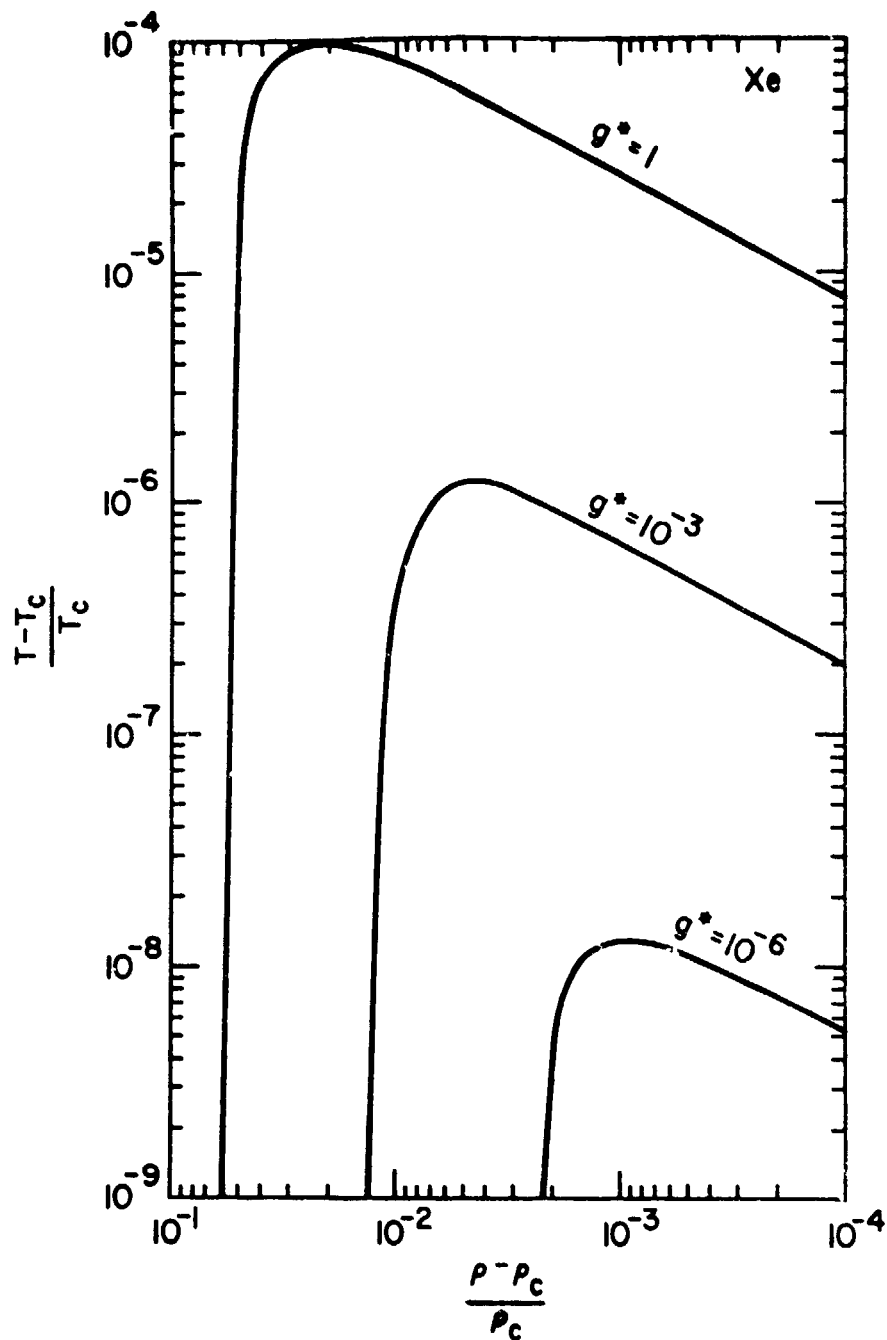
$$\tau^{-1} \geq \left(\frac{10}{x}\right) \zeta. \tag{2.4.16}$$

49

Fig. 2.10. Contours of $\frac{1}{\xi}\frac{d\xi}{dz}$ h = p for xenon with h = 100μm, p = .01. Experiments with a 100μm diameter beam in the region below and to the right of each contour are severely affected by averaging over correlation lengths at the values of g* indicated.

50

This is least restrictive for large x. The condition (2.4.16) gives a lower bound for r which is converted into ΔT^* for $\Delta\rho^* = 0$ and $\Delta\rho^*$ for $\Delta T^* = 0$. Table 2.4.4 gives the results for $\lambda = 6328\text{Å}$ and $\lambda = 3.391\mu m$ for the case x = 1. Note they are independent of g.

Table 2.4.4

Scattering vector approach bounds

λ	$r = \Delta T^*$ $(\Delta\rho^* = 0)$	$\Delta\rho^*$ $(\Delta T^* = 0)$
6328Å	6.3×10^{-7}	6.6×10^{-3}
3µm	1.6×10^{-8}	1.8×10^{-3}

The results in Table 2.4.4 indicate that the change in wavelength from 6328 to 3µm would keep the smearing of k to an acceptable limit down to the turbidity/multiple scattering limit for ℓ of the order of 10^{-3} m or 10^{-4} m.

We can summarize the results reported here by stating that with the most favorable geometry of 100µm path cells and 3µm radiat' n light scattering experiments could approach closer to the critical point by 10^3 in r corresponding to 10^3 in ΛT^* and 10^1 in $\Delta\rho^*$ in a 10^{-3}g environment. At present, experimental limitations would prevent us from fully utilizing the minimum accelerations of 10^{-6}g. Even at 3µm a requirements remains from $\frac{d\xi}{dz}$ to achieve the minimum r allowed by density and turbidity we must fill the cell accurately to ρ_c to within .02%. This is certainly possible but requires more care than does sample loading for earth bound experiments.

3. **Limitations in critical-region experiments due to modifications of**

   fluid properties by a gravitational field.

   In the preceding sections we have commented on the technical complications
   that are encountered in various experimental methods near the critical
   point of a fluid in a gravitational field. However, in addition,
   intrinsic limitations in earth-bound experiments exist due to the fact
   that the gravitational field modifies the fluid properties in the immediate
   vicinity of the critical point.

   As mentioned in Section 2.4, upon approaching the critical point the
   increase of the compressibility is accompanied by an increase in the
   size of the fluctuations that extend over a correlation length ξ. If
   the system were homogeneous and in true thermodynamic equilibrium the
   compressibility and, hence, the correlation length would actually diverge
   at the critical point. However, the presence of the gravitational field
   prevents the fluctuations from growing indefinitely and compressibility
   and correlation length will in fact remain finite. Thus the presence of
   the gravitational field causes round off effects which change the
   nature of the thermodynamic behavior in the immediate vicinity of the
   critical point. It is the purpose of this Section to estimate the range
   in temperature and density where experiments will be affected by these
   round off phenomena and to elucidate how this range depends on the
   magnitude of the gravitational field.

   As explained in Section 2.2 the gravitational field induces a
   density gradient in a fluid near the critical point. When the density
   does not change too rapidly as a function of height, one may assume that

the local thermodynamic properties of the fluid at a given level are the
same as that of a macroscopic homogeneous system with the same values of
density and temperature. Under these conditions the density profile is
determined by the equations given in Appendix B and measurements of the
local fluid properties in a gravitational field does provide information
on the thermodynamic behavior of a homogeneous fluid in the absence of
a gravitational field.

The assumption of local thermodynamic equilibrium is justified when
the fluid is locally homogeneous over distances of the order of the
correlation length, but will break down when the fluid properties begin
to vary over distances of the order of the correlation length. In
Fig. 3.1 we show calculated density profiles for xenon in the earth's
gravitational field at three reduced temperatures, namely $\Delta T^* = 10^{-4}$,
10^{-6} and 10^{-8}. The existence of a density gradient implies that also the
correlation length ξ varies as a function of the height. In Fig. 3.2 we
show the correlation length ξ as a function of the height for xenon in
the earth's gravitational field. The curves are calculated in the
approximation that the assumption of local thermodynamic equilibrium
remains valid. However, in the dashed part of the curves the correlation
length varies so rapidly that the system can no longer assume local
equilibrium states that are homogeneous over the range of ξ. Under
these conditions the laws of thermodynamics no longer suffice to specify
the nature of the equilibrium states. The complications that arise when
the macroscopic thermodynamic relations can no longer be applied at the
local level, will be referred to as non local effects.

Such effects will enter when the correlation length ξ starts to
vary over its own height $h = \xi$. It thus follows from (C.19) that for
measurements conducted with precision p non local effects will be encountered
when
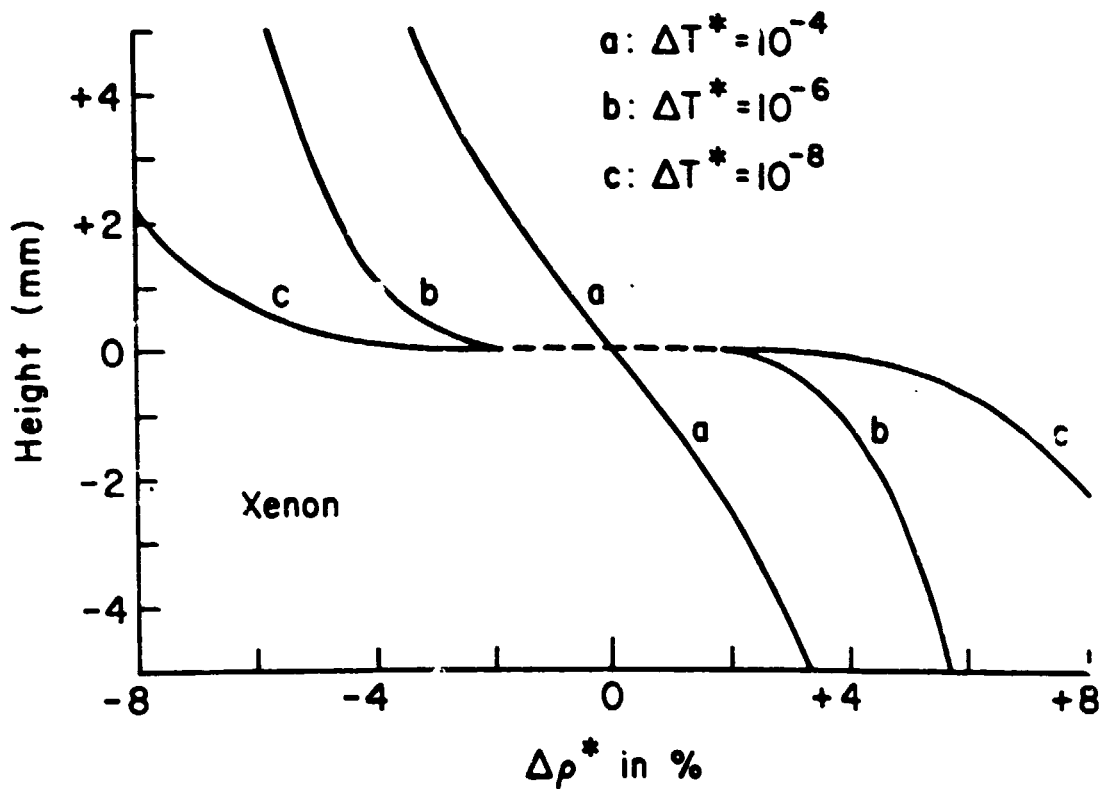
Fig. 3.1 Calculated density profiles for xenon in the earth's gravitational
field and assuming local thermodynamic equilibrium. In the dashed
part of the curves the density varies so rapidly that the assumption
of local thermodynamic equilibrium no longer applies.

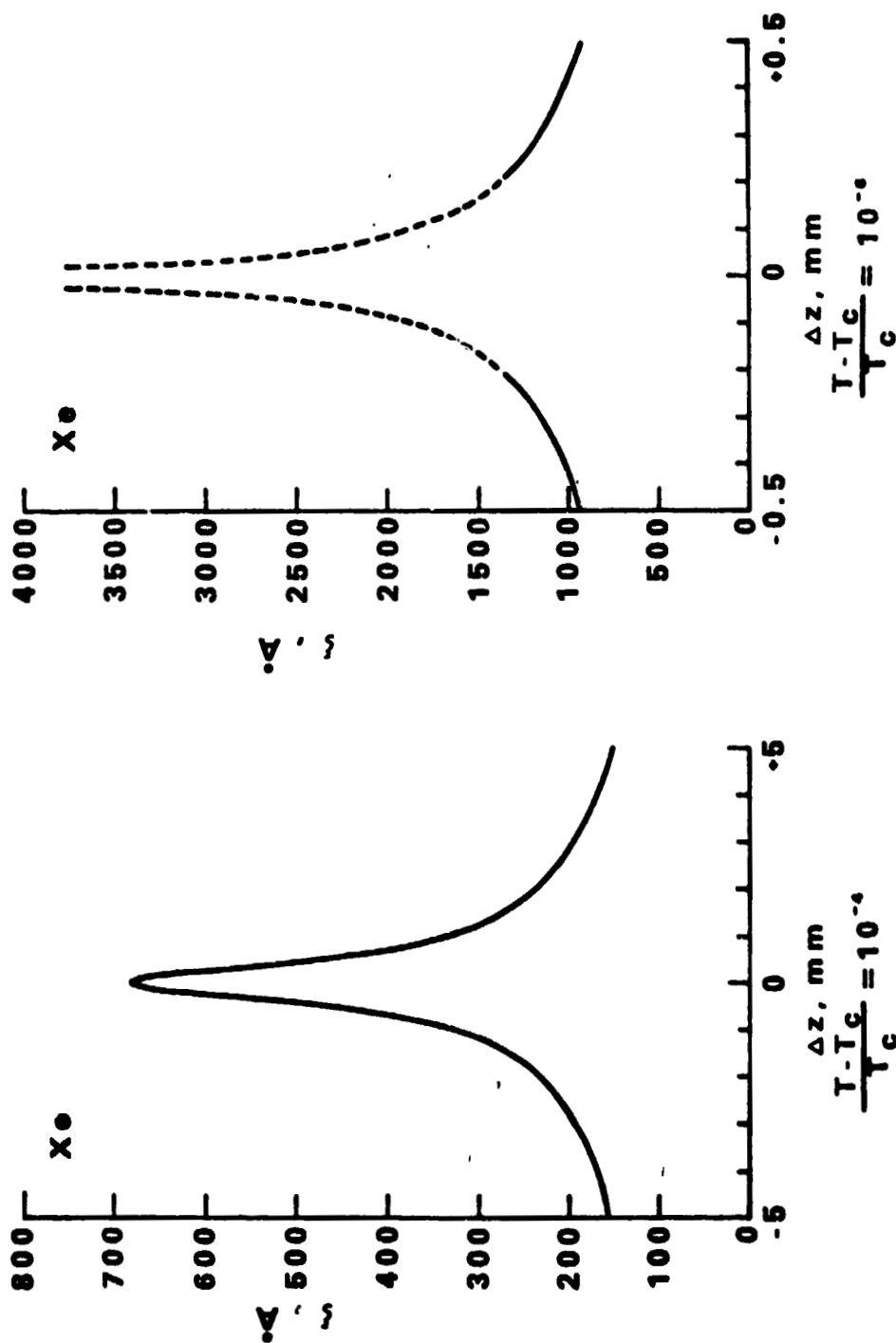Fig. 3.2 Correlation length ξ as a function of height for xenon in the earth's gravitational field if one assumes local thermodynamic equilibrium. In the dashed part of the curve this assumption breaks down and the actual range of the fluctuations will be suppressed due to non local effects.

$$\left(\frac{\partial \xi}{\partial z}\right)_T \geq p \tag{3.1}$$

In terms of the parameters r and θ of the restricted cubic model equation of state, it follows from (C.16) that non local effects can be avoided only if

$$r^{\nu+\beta\delta}(\theta) \geq \left(\frac{g^*}{p\ H_0}\right)\left(\frac{\nu\xi_0}{a_2}\right)\left[-\frac{2b_2^2\theta^2}{2\beta\delta b_2^2\theta^2(1-\theta^2)+(1-3\theta^2)(1-b_2^2\theta^2)}\right] \tag{3.2}$$

Using the xenon parameters given in Appendix E, we conclude that at the critical temperature, $\Delta T^* = 0$ ($\theta = \pm b_2^{-1}$), non local effects will be encountered unless

$$|\Delta\rho^*| \geq 0.007 \left(\frac{g^*}{p}\right)^{\frac{\beta}{\nu+\beta\delta}} = 0.007 \left(\frac{g^*}{p}\right)^{0.163} \tag{3.3}$$

In Fig. 3.3 we indicate the region in the $\Delta T^* - \Delta\rho^*$ plane where the behavior of the fluid is modified by non local effects and, hence, where its properties will be fundamentally different from a fluid in the absence of gravity.

Near the critical isochore, $\Delta\rho^* = 0$, condition (3.1) becomes unrealistic because of the rapid variation of $\partial\xi/\partial z$ and we should, instead, consider the integrated form

$$\frac{\Delta\xi}{\xi} \leq p \tag{3.5}$$

The distance Δz_p over which the change in ξ is smaller than p is derived in Appendix C. In particular we require

56
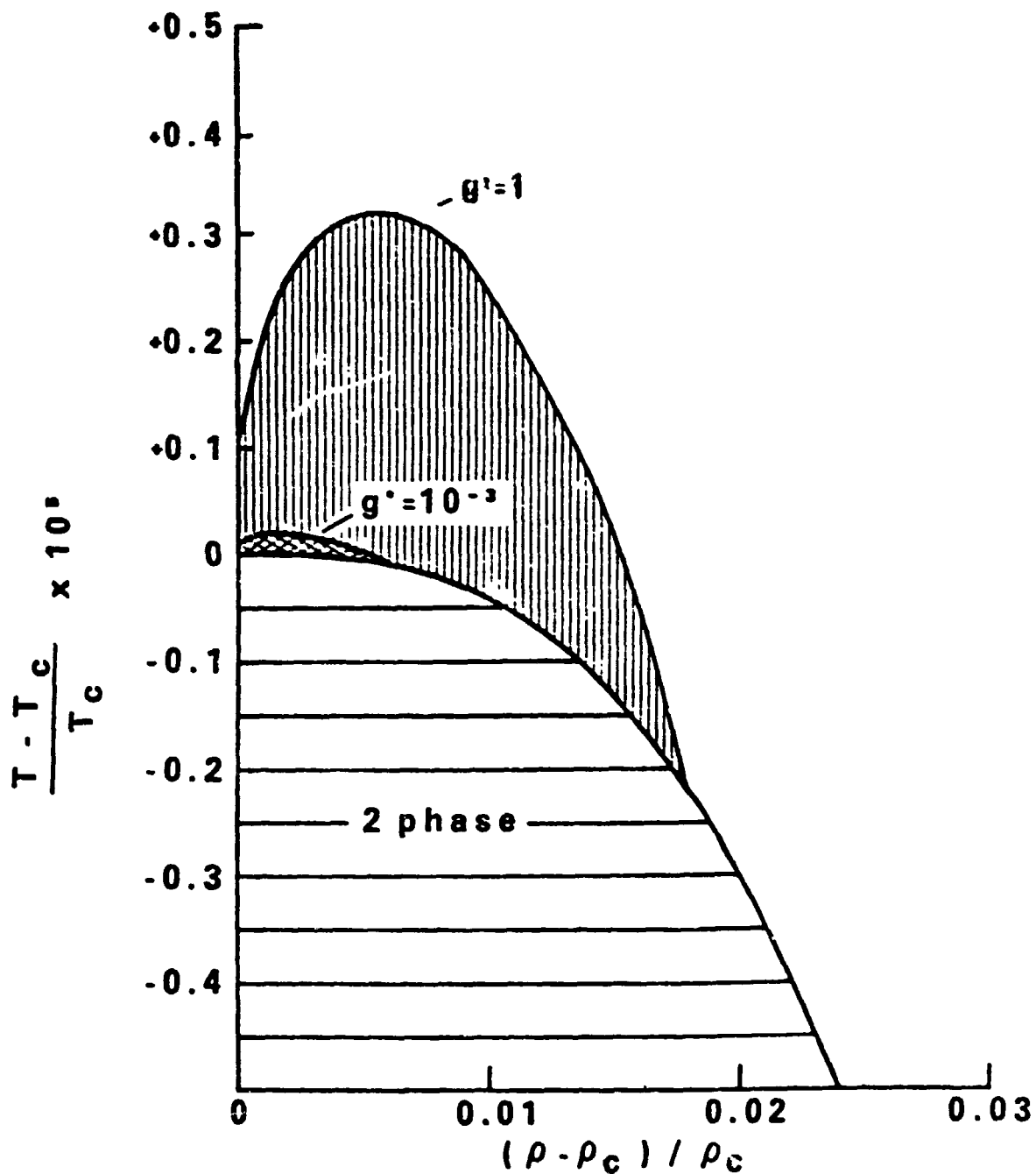
Fig. 3.3 Region in the temperature-density plane where the fluid properties are modified by non local effects for $g* = 1$ (earth's gravitational field) and $g* = 10^{-3}$ The curves refer to experiments for xenon with a precision at the 1% level ($p = 10^{-2}$).

57

$$\xi = \xi_0 |\Delta T^*|^{-\nu} \ll 2\Delta z_\rho \tag{3.6}$$

where Δz_p is defined in (C.13). For xenon we obtain

$$|\Delta T^*| \geq 0.4 \times 10^{-6} \left(\frac{g^*}{\sqrt{\rho}}\right)^{\frac{1}{\nu+\beta\delta}} = 0.4 \times 10^{-6} \left(\frac{g^*}{\sqrt{\rho}}\right)^{0.46} \tag{3.7}$$

This equation determines the intercept of the contourr in Fig. 3.3 with the ΔT^* axis.

It follows from (C.11a) and (3.2) that the system will only satisfy the conditions for local thermodynamic equilibrium when

$$\xi \leq 1.5 \times 10^{-6} \left(\frac{\rho}{g^*}\right)^{\frac{\nu}{\nu+\beta\delta}} m = 1.5 \times 10^{-6} \left(\frac{\rho}{g^*}\right)^{0.29} m \tag{3.8}$$

When the critical point is approached more closely, the increase of the range of the fluctuations will be suppressed by non local effects. It seems plausible to assume that the correlation length ξ in a fluid in a gravitational field cannot grow any further when $(\partial\xi/\partial z)_T \gtrsim 1$ in the local equilibrium approximation. Hence, in a fluid in a gravitational field, the correlation length will always remain finite and of the order of

$$\xi \leq \xi_{max} \simeq 1.5 \times 10^{-6} g^{*-0.29} m \tag{3.9}$$

It should be noted that the maximum correlation length attainable will only increase inversely proportional to the cube root of the gravitational field.

In this section we have considered the intrinsic limitations of thermodynamic experiments near the critical point of a fluid in a gravitational field. At present, more stringent limitations are imposed by the complications associated with the state of the art of the various available experimental methods. Nevertheless, current experimental techniques have developed to the point that they are on the verge of reaching the region of these intrinsic limitations in earth-bound experiments.

4. Conclusions

In this report we have shown that gravity causes experiments to become inaccurate when the critical point is approached sufficiently closely. We have considered the ranges in ΔT^* and Δp^* which are inaccessible in a variety of earthbound experiments and how these ranges shrink when gravity is reduced. Some of our conclusions are summarized numerically in Table 4.1.

The critical point is a focal point of anomalous behavior of many physical properties. In order to understand the nature of these anomalies it is desirable to approach the critical point as closely as possible. In fact, the most recent experiments (Hocken and Moldover, 1976; Balzarini and Ohrn, 1972) indicate that at temperatures as close a 1 mK from the critical temperature the anomalous behavior near the critical point of fluids, although appearing to approach Ising mode' behavior still differs from the behavior predicted by some theories for that model. A disappearance of this difference at the critical point would have considerable theoretical significance.

Experiments in a low-g environment will provide opportunities to study the nature of the anomalies in a range of temperatures near the critical temperature inaccessible in earthbound experiments. To discuss which anomalies are best suited for study in space, it is convenient to classify anomalies as "strong" and "weak" (Griffiths and Wheeler, 1970). In this rough classification, quantities which behave like $(T-T_c)^{-p}$ on the critical isochore are called strongly anomalous if p is greater than, perhaps, 0.5. Thus the isothermal compressibility, the constant pressure specific heat, the thermal diffusivity, and the correlation length exhibit strong anomalies in pure fluids. In contrast,

60

Table 4.1 Limitations imposed by gravity on critical-region experiments

Experiment	Property	Characteristic length	Nature of limitation	Excluded range on earth		Excluded range at $10^{-3} g_0$		Excluded range at $10^{-6} g_0$	
				$\rho - \rho_c$ / ΔT^*	$T - T_c$ / ΔT^*	$\rho - \rho_c$ / ΔT^*	$T - T_c$ / ΔT^*	$\rho - \rho_c$ / ΔT^*	$T - T_c$ / ΔT^*
PVT	Density	Cell 1 cm high	Density gradient	6×10^{-4}	8×10^{-2}	2×10^{-6}	1×10^{-2}	6×10^{-9}	1×10^{-3}
Float densimeter	Density	Height of float 2.5 mm	Density gradient	2×10^{-4}	5×10^{-2}	1×10^{-6}	6×10^{-3}	3×10^{-9}	6×10^{-4}
Capacitance	Density	Spacing between plates 0.2 mm	Density gradient	2×10^{-5}	2×10^{-2}	7×10^{-8}	3×10^{-3}	2×10^{-10}	4×10^{-4}
Calorimetry	Heat capacity	Cell 1 cm high	Redistribution of matter	3.5×10^{-4}	6×10^{-2}	4×10^{-6}	1×10^{-2}	5×10^{-8}	3×10^{-3}
Refractive index	Compressibility	Path in cell 3 mm	Curved path of beam in cell	1.5×10^{-5}	2×10^{-2}	N.A.	N.A.	N.A.	N.A.
Light (6328 Å) scattering	Compressibility	Path in cell 3mm	Turbidity	5×10^{-5}	3×10^{-2}	5×10^{-5}	3×10^{-2}	5×10^{-5}	3×10^{-2}
	correlation length	Height of scattering volume 0.1 mm	correlation length gradient	2×10^{-5}	6×10^{-2}	2×10^{-7}	1×10^{-2}	3×10^{-9}	2×10^{-3}
All	Any	Correlation length	Non local effects	1.5×10^{-6}	1.5×10^{-2}	7×10^{-8}	4×10^{-3}	3×10^{-9}	2×10^{-4}

The estimates refer to xenon in the earth's gravitational field when the indicated property is to be measured within it.

61

properties for which p is less than 0.5 (or even negative) exhibit weak anomalies. Examples in pure fluids are: the velocity of sound, the constant volume specific heat, the dielectric constant, and the shear viscosity.

In general, strongly anomalous quantities can be studied sufficiently well on earth (particularly with refinements of optical techniques mentioned in Chapter 2) so that low-g experiments do not seem desirable at present. If the technology advances to the point where the non local effects of Chapter 3 are encountered, this statement would have to be revised. On the other hand, those properties which exhibit weak anomalies and which must be studied in bulk samples are excellent candidates for scientifically valuable low-g experiments. The study of these weak anomalies in pure fluids is hampered by the strong variation of fluid density with height on earth.

The weak anomaly in the index of refraction is a particularly important one for low-g studies. Thorough understanding of the index of refraction anomaly is of interest in itself; however, it is of even greater interest in its impact upon the interpretation of equation of state data obtained by optical techniques. Other good candidates for study in a low-g environment are the C_v and viscosity anomalies which, with present technology, must be studied in bulk samples at least several tenths of a millimeter high.

In the areas of phase transition phenomena in fluids, low-g studies of spinodal decomposition, nucleation, and macroscopic phase separation all seem appropriate. At this time, it is hard to present a detailed justification of low-g studies because the phenomenology is not as well developed in these areas as it is for the thermophysical properties. We

62

believe exploratory experiments which exploit the long sedimentation times available in spacelab are appropriate. We agree with the Overstudy Committee (Dodge et al., 1975) that very simple experiments will be extremely important. The Overstudy Committee described one such experiment (Dodge et al., p.9) which we heartily endorse:

Take a set of samples of a one-component fluid with different densities. Included should be a sample at subcritical density, a sample at the critical density and a sample at supercritical density. Let the temperature vary either continuously or discontinuously through the transition temperature and take photographs at regular temperature intervals. Compare these photographs with those obtained at earth under the same instrumental conditions. Conduct similar experiments for a set of samples of a binary mixture at concentrations smaller than, equal to and larger than the critical concentration.

Appendix A. <u>Parametric equations of state for fluids near the critical point</u>.

A.1 Introduction

Let ρ be the density, V the volume, P the pressure, T the temperature, μ the chemical potential, $K_T = \rho^{-1}(\partial\rho/\partial P)_T$ the isothermal compressibility and C_V the heat capacity at constant volume. It will also be convenient to introduce a "symmetrized" compressibility

$$X_T = (\partial\rho/\partial\mu)_T = \rho^2 K_T \qquad \text{(A.1)}$$

The thermodynamic properties are made dimensionless by expressing them in units of appropriate combinations of the critical temperature T_c, the critical density ρ_c and the critical pressure P_c. Specifically, we define

$$T^* = T/T_c, \; \rho^* = \rho/\rho_c, \; P^* = P/P_c$$

$$\text{(A.2)}$$

$$\mu^* = \mu\rho_c/P_c, \; X_T^* = X_T P_c/\rho_c^2, \; C_V^* = C_V T_c/V P_c$$

Note that the reduced specific heat C_V^* is taken per unit volume. In addition we define the differences

$$\Delta\mu^* = \{\mu(\rho,T) - \mu(\rho_c,T)\}\rho_c/P_c \qquad \text{(A.3a)}$$

$$\Delta T^* = (T-T_c)/T_c \qquad \text{(A.3b)}$$

$$\Delta\rho^* = (\rho-\rho_c)/\rho_c \qquad \text{(A.3c)}$$

64

The behavior of various thermodynamic properties is described by power laws when the critical point is approached along specific paths in the $\Delta T^* - \Delta \rho^*$ plane. One customarily defines four critical exponents α, β, γ, and δ associated with the thermodynamic behavior of fluids near the critical point. (Rowlinson, 1969). The exponent α describes the divergence of C_V along the critical isochore.

$$(T \geq T_c, \rho = \rho_c) \qquad C_V^*/T^* = \frac{A}{\alpha} \{(\Delta T^*)^{-\alpha} - 1\}, \qquad (A.4a)$$

the exponent β characterizes the shape of the coexistence curve

$$(T \leq T_c, \rho = \rho_{cxc}) \qquad \Delta \rho_{cxc}^* = \pm B |\Delta T^*|^\beta, \qquad (A.4b)$$

the exponent γ describes the divergence of the compressibility

$$(T \geq T_c, \rho = \rho_c) \qquad \chi_T^* = \Gamma (\Delta T^*)^{-\gamma} \qquad (A.4c)$$

and the exponent δ specifies the behavior of $\Delta \mu$ along the critical isotherm

$$(T = T_c) \qquad \Delta \mu^* = D (\Delta \rho^*) |\Delta \rho^*|^{\delta - 1} \qquad (A.4d)$$

The description of the thermodynamic behavior is based on a scaling hypothesis (Widom, 1965; Fisher, 1967; Levelt Sengers, 1974, 1975). This scaling hypothesis suggests that the equation of state upon approaching the critical point will be asymptotically of the form (Griffiths, 1967)

$$\Delta\mu^\star = \Delta\rho^\star \left|\Delta\rho^\star\right|^{\delta-1} h(x) \qquad (A.5)$$

$$x = \Delta T^\star / \left|\Delta\rho^\star\right|^{1/\beta} \qquad (A.6)$$

The scaling hypothesis implies that the thermodynamic critical exponents introduced in (A.4) satisfy the relations

$$2 - \alpha = \beta(\delta+1)$$
$$\gamma = \beta(\delta-1) \qquad (A.7)$$

so that only two exponents can be chosen independently.

The function $h(x)$ in (A.5) must satisfy a number of stability and analyticity conditions (Griffiths, 1967). However, it turns out to be very difficult to formulate an explicit mathematical expression for the function of $h(x)$ that would satisfy all required analyticity conditions and which would be analytically integrable to calculate the specific heat (Vicentini-Missoni et al., 1969; Schmidt, 1971; Levelt Sengers et al., 1976).

These problems are solved by using parametric equations of state (Josephson, 1969; Schofield, 1969). In the parametric equations of state the relationship between the physical variables $\Delta\mu^\star$, $\Delta T^\star$ and $\Delta\rho^\star$ is given implicitly via two parametric variables r and θ. The constraint that the scaling law (A.5) is satisfied is met by the following choice

66

$$\Delta\mu^* = r^{\beta\delta} H(\theta)$$

$$\Delta T^* = r\ T(\theta) \qquad\qquad (A.8)$$

$$\Delta\rho^* = r^{\beta} M(\theta)$$

The variable r is meant, in some sense, to describe a distance from the critical point and the azimuthal variable θ a location on a contour of constant r. The critical isochore, the critical isotherm and the coexistence curve are all curves of constant angle θ. In Fig. A1 we show the location of these curves in the $\Delta\mu^*$ - ΔT^* plane and indicate the meaning of the parametric variables r and θ.

Parametric equations of state with various choices for the functions $H(\theta)$, $T(\theta)$ and $M(\theta)$ have been used successfully to represent experimental equation of state data in the critical region of fluids. The parametric equations of state used in this report are the restricted linear model, the restricted cubic model and the Wilcox-Estler equation of state.
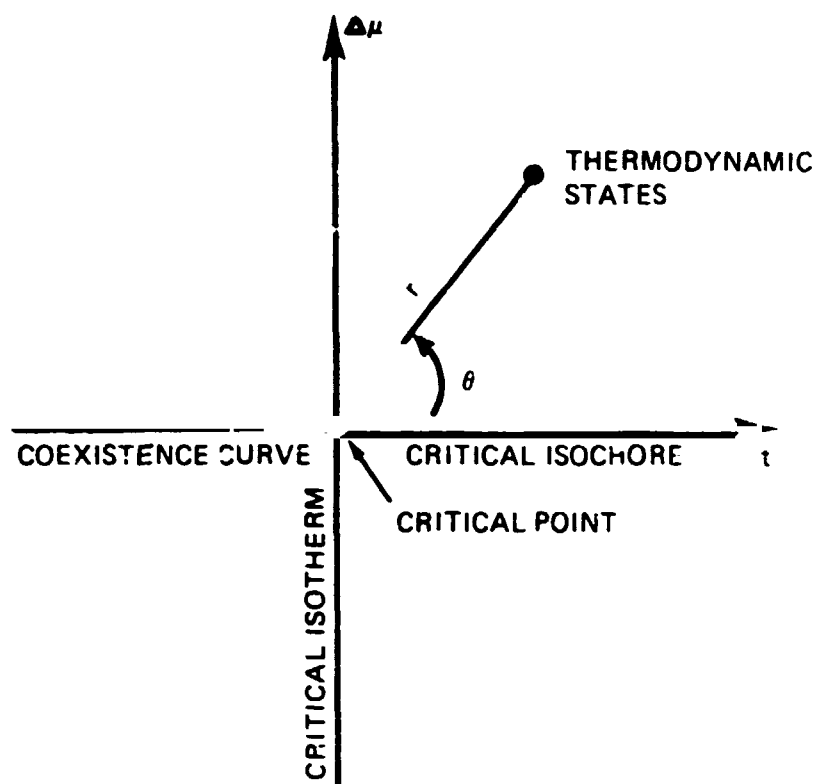
Fig. A1. Coexistence curve, critical isochore and critical isotherm in
the plane with coordinate axes $\Delta\mu$ and $t = \Delta T^*$.

A.2 Restricted linear model.

The restricted linear model equation of state corresponds to the choice (Schofield, 1969; Schofield, Litster and Ho, 1969)

$$\Delta\mu^* = a_1 \, r^{\beta\delta}\theta(1-\theta^2) \tag{A.9a}$$

$$\Delta T^* = r(1-b_1^{\;2}\theta^2) \tag{A.9b}$$

$$\Delta\rho^* = k_1 \, r^{\beta}\theta \tag{A.9c}$$

with

$$b_1^{\;2} = \frac{\delta-3}{(\delta-1)(1-2\beta)} \tag{A.9d}$$

where a_1 and k_1 are adjustable constants. In this formulation $\theta = 0$ on the critical isochore. $\theta = \pm 1/b_1$ on the critical isotherm and $\theta = \pm 1$ on the coexistence curve. The sign of θ corresponds to the sign of $\Delta\rho^*$.

The restricted linear model yields for the compressibility

$$\chi_T^{*-1} = \left(\frac{a_1}{k_1}\right)r^{\gamma}\left[1 + \left(\frac{2\beta\delta-3}{1-2\beta}\right)\theta^2\right] \tag{A.10}$$

and for the singular contribution to the specific heat

$$\frac{c_{v,sing}^*}{T^*} = a_1 k_1 \frac{(1-2\beta)(\gamma-1)(\delta-1)}{2\alpha(\delta-3)} r^{-\alpha} \tag{A.11}$$

so that a contour of constant r may be interpreted as a contour of constant anomalous specific heat (Schofield, Litster and Ho, 1969).

The restricted linear model has been used to fit experimental data for magnets (Schofield, Litster and Ho, 1969) and fluids (Hohenberg and

Barmatz, 1972; Huang and Ho, 1973; Thoen and Garland, 1974; White and
Maccabee, 1975; Levelt Sengers and Sengers, 1975; Levelt Sengers et al.,
1976). It can be integrated and also be fitted to the pressure (Murphy
et al., 1973, 1975).

Restricted linear model parameters for a variety of fluids are
presented in Appendix D.

A.3 Restricted cubic model.

The restricted cubic model equation of state corresponds to the
choice (Ho and Litster, 1970; Huang and Ho, 1973)

$$\Delta\mu^* = a_2 \; r^{\beta\delta} \; \theta(1-\theta^2) \tag{A.12a}$$

$$\Delta T^* = r(1-b_2^2 \; \theta^2) \tag{A.12b}$$

$$\Delta\rho^* = k_2 \; r^\beta \; \theta(1+c \; \theta^2) \tag{A.12c}$$

with

$$b_2^2 \; = \frac{3}{3-2\beta} \; , \; c = \frac{2\beta\delta-3}{3-2\beta} \tag{A.12d}$$

where a_2 and k_2 are adjustable constants. Just as in the linear model,
$\theta = 0$ on the critical isochore, $\theta = \pm 1/b_2$ on the critical isotherm and
$\theta = \pm 1$ on the coexistence curve.

The restricted cubic model yields for the compressibility the
simple form

$$X_T^* = \frac{k_2}{a_2} \; r^{-\gamma} \tag{A.13}$$

so that a contour of constant r corresponds to a contour of constant
compressibility.

When the restricted cubic model is fitted to experimental data the
quality of the representation is comparable to that of the restricted
linear model. Restricted cubic model parameters for a variety of fluids
are presented in Appendix D.

A.4 Wilcox-Estler model.

The parametric equation introduced by Wilcox and Estler [1971] has
been used to analyze density gradient profiles in the extreme vicinity
of the critical point (Estler et al., 1975; Hocken and Moldover, 1976).
It is defined through the equations

$$\Delta\mu^* = \frac{\beta}{\gamma} r^\gamma Y^\beta(r,\theta)H(\theta) \tag{A.14a}$$

$$\Delta T^* = r\theta \tag{A.14b}$$

$$\Delta\rho^* = Y^\beta(r,\theta) \left[1 + \frac{\beta}{\gamma} W(\theta)\right] \tag{A.14c}$$

with

$$W(\theta) = \frac{1 - \theta/\theta_x}{1 - \theta/\theta_0} \tag{A.14d}$$

$$Y(r,\theta) = Y_0 r (1-\theta/\theta_0)^\Delta \tag{A.14e}$$

$$\Delta = 1 - \theta_0/\theta_x \tag{A.14f}$$

This equation of state is designed such that

$$\chi_T^* = r^{-\gamma} \tag{A.15}$$

so that a contour of constant $r = (1/\chi_T^*)^{1/\gamma}$ corresponds to a contour of

71

constant compressibility as in the restricted cubic model. It has the additional feature that ΔT^* is a linear function of both r and θ.

In this formulation lines of constant θ are straight lines as indicated in Fig. A2. In this model $\theta = o$ corresponds to the critical _isotherm_, while $\theta = \theta_o$ on the critical isochore and $\theta = \theta_x$ on the coexistence boundary. For the special choice $\beta\Delta = 3/2$ the Wilcox-Estler model reduces to the restricted cubic model (Estler _et al_., 1975).
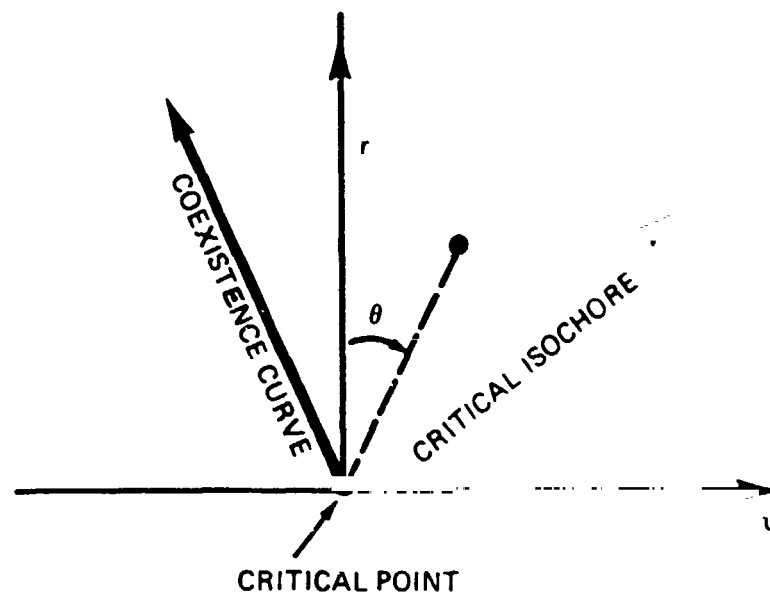
Fig. A2. Coexistence curve, critical isochore and critical isotherms in the
plane with coordinate axis $r = (1/x_T^*)^{1/\gamma}$ and $t = \Delta T^*$.

Appendix B.   Calculation of density profile.

We assume that at each level z the local chemical potential $\mu(\rho(z),T)$ equals tne chemical potential of a system with uniform density $\rho = \rho(z)$ at temperature T in the absence of gravity. The conditions under which this assumption is valid are discussed in Section 3 of this report. Since in the presence of gravity the total chemical potential is the sum of the local chemical potential $\mu(\rho(z),T)$ and the gravitational potential mgz, we have

$$\mu(\rho(z),T) - \mu(\rho(z_0),T) = - mg\Delta z \qquad (B.1)$$

where m is the molecular mass, if the chemical potential is taken per particle and where $\Delta z = z - z_0$. For convenience we take the reference level z_c as the level where $\rho = \rho_c$. In terms of dimensionless quantities we write

$$\Delta z = - H \Delta\mu^* \qquad (B.2)$$

with

$$H = P_c/(\rho_c\, mg) \qquad (B.3)$$

The quantity $\Delta\mu^*$ is defined in (A.3a) and the product $\rho_c m$ is the mass density at the critical point. The quantity H represents a scale height for the chemical potential of a fluid in a field of gravity g. H_0 represents the scale height for the chemical potential in the earth's gravitational field where $g = g_0$. In Appendix D we present the scale factors for the critical isotherm for a number of fluids in the earth's gravitational field, where

74

$$D \ H_o = DP_c/\rho_c \ mg_o \qquad (B.4)$$

(These scale factors for the critical isotherm differ from H_o by a numerical factor, D, which varies between 1.2 and 3.2 among various fluids). Introducing a gravity ratio

$$g^* = g/g_o \qquad (B.5)$$

we may rewrite (B.2) as

$$\Delta z = - \left(\frac{H_o}{g^*} \right) \Delta \mu^* \qquad (B.6)$$

Substitution of the scaled equation of state (A.5) into (B.6) yields the relationship between height and density at a given temperature. In practice we either use the restricted linear model (A.9), the restricted cubic model (A.12), or the Wilcox-Estler model (A.14).

It follows from (A.1) and (B.6) that the density gradient $(\partial \rho^*/\partial z)_T$ is given by

$$\left(\frac{\partial \rho^*}{\partial z} \right)_T = - \frac{g^*}{H_o} \left(\frac{\partial \rho^*}{\partial \mu^*} \right)_T = - \frac{g^*}{H_o} \chi_T^* \qquad (B.7)$$

In practice the density can be determined as a function of height using a float densimeter (Greer et al., 1974) or by measuri. the capacitances between a stack of horizontal conduction plates (Weber, 1970). The density resolution in such experiments is limited by the variation of the density over the height h of the float or the distance h between the two capacitor plates. If the local density is to be obtained with a precision p we must require that

$$\left|\rho^*(\Delta z + h/2) - \rho^*(\Delta z - h/2)\right| \approx h\left|\frac{\partial \rho^*}{\partial z}\right| \leq p \qquad (B.8)$$

It thus follows from (B.7) that errors due to gravity in determining densities are avoided if

$$x_T^* \leq \frac{H_0 p}{g^* h} \qquad (B.9)$$

or in terms of the cubic model parameters, using (A.13),

$$r \geq \left(\frac{g^* h}{H_0 p} \frac{h_2}{a_2}\right)^{1/\gamma} \qquad (B.10)$$

For xenon this condition reads

$$r \geq 6.2 \times 10^{-4} \left(\frac{g^* h}{p}\right)^{0.84} \qquad (B.11)$$

where the height h is to be expressed in m. In particular at the critical isochore $\rho = \rho_c$

$$\Delta T^* \geq 6.2 \times 10^{-4} \left(\frac{g^* h}{p}\right)^{0.84} \qquad (B.12)$$

and at the critical isotherm $T = T_c$

$$\Delta \rho^* \geq 0.076 \left(\frac{g^* h}{p}\right)^{0.3} \qquad (B.13)$$

76

Appendix C. Calculation of correlation length.

C.1. Definition of correlation length.

When a fluid approaches the gas-liquid critical point, its thermodynamic state is accompanied by large fluctuations in the density. The magnitude and spatial character of these fluctuations are described in terms of a correlation function defined as (Stanley, 1971)

$$\rho^2 G(|\vec{R}-\vec{R}'|) = <\rho(\vec{R})\rho(\vec{R}') > - \rho^2 \qquad (C.1)$$

where $\rho(\vec{R})$ is the local (number) density at position $\vec{R}$ and ρ the average equilibrium density which is independent of the position $\vec{R}$ (not considering the presence of external forces such as gravity). The zeroth order moment of the correlation function is related to the isothermal compressibility by the fluctuation theorem

$$k_B T \; \chi_T = \rho^2 \int d\vec{R} \; G(R) \qquad (C.2)$$

The correlation function $G(R) = G(\Delta\rho^*, \Delta T^*; R)$ is a function $\Delta\rho^*$ and ΔT^* as well as of R (where $R = |\vec{R} - \vec{R}'|$).

The spatial extent of the fluctuations is characterized by a correlation length ξ. It is defined as (Fisher, 1964, 1967)

$$\xi^2 = \frac{1}{6} \; \frac{\int d\vec{R} \; R^2 \; G(R)}{\int d\vec{R} \; G(R)} \qquad (C.3)$$

The correlation length ξ diverges at the critical point. In particular along the critical isochore it follows the power law

$$(T \geq T_c, \rho = \rho_c) \qquad\qquad \xi = \xi_o (\Delta T^*)^{-\nu} \qquad (C.4)$$

77

Another exponent η is introduced to specify the nature of the dependence of the correlation function on the distance R. It is defined such that at the critical point $\Delta\rho^* = 0$, $\Delta T^* = 0$

$$G(o,o;R) \propto \frac{1}{R^{1+\eta}}$$

The exponent is zero in the classical theory of Ornstein and Zernike (Fisher, 1964). In current theories η is small, but finite.

The correlation function exponents ν and η are related to the thermodynamic critical exponents α, β, γ, δ introduced in Appendix A by the relations (Fisher, 1967; Widom, 1974)

$$\gamma = \nu(2-\eta) \tag{C.6}$$

$$3\nu = 2-\alpha \tag{C.7}$$

$$\frac{2-\eta}{3} = \frac{\delta-1}{\delta+1} \tag{C.8}$$

The relations (C.7) and (C.8) are sometimes referred to as hyperscaling relations (Levelt Sengers and Sengers, 1975).

C.2 Correlation length as a function of density and temperature.

The correlation length $\xi = \xi(\Delta\rho^*, \Delta T^*)$ is a function of density and temperature. The hypothesis of scaling for the thermodynamic behavior can be extended to the correlation function $G(\Delta\rho^*, \Delta T^*; R)$ as a function of $\Delta\rho^*$, ΔT^* and R (Kadanoff, 1966). The scaling hypothesis implies that the correlation length ξ can be written in the form (Sengers and Levelt Sengers, 1976)

$$\xi = \xi_0 \; \hat{R}(x/x_0) \; (\Gamma^{-1} \; \chi_T^*)^{\frac{1}{2-\eta}} \qquad (C.9)$$

where $x = \Delta T^*/|\Delta\rho^*|^{1/\beta}$ is the thermodynamic scaling variable introduced in (A.6) and $x_0 = -\Delta T^*/|\Delta\rho_{cxc}^*|^{1/\beta} = B^{-1/\beta}$, where B is the amplitude of the power law (A.4b) for the coexistence curve. The function $\hat{R}(x/x_0)$ is a universal function such that $\hat{R}(\infty) = 1$ at the critical isochore $x = \infty$. The amplitude ξ_0 can be deduced from light scattering data (Chu, 1972).

In this report we have calculated the correlation length in the approximation that $\hat{R}(x/x_0) = 1$ independent of x

$$\xi = \xi_0 \; (\Gamma^{-1} \; \chi_T^*)^{\frac{1}{2-\eta}} \qquad (C.10)$$

This approximation, though not strictly valid, is adequate for the purpose of this report (Senger and Levelt Sengers, 1976). In this approximation a contour of constant compressibility χ_T^* coincides with a contour of constant correlation length ξ. For this reason we found it convenient to calculate ξ using the restricted cubic model equation of state (A.12) for which

79

$$\xi = \xi_0 \ r^{-\nu} \tag{C.11a}$$

$$\Delta T^* = r(1 - b_2^2 \ \theta^2) \tag{C.11b}$$

$$\Delta \rho^* = k_2 \ r^\beta \ \theta(1 + c \ \theta^2) \tag{C.11c}$$

with b_2 and c again given by (A.12d).

C.3 Correlation length as a function of height.

Once the density profile and density gradient profile has been calculated from (B.6) and (B.7), the correlation length as a function of height follows from (C.10). In terms of the parameters of the restricted cubic model the relationship between the correlation length ξ and the height z at a given temperature ΔT^* is determined by

$$\xi = \xi_0 \; |\Delta T^*|^{-\nu} \; |1 - b_2^2 \; \theta^2|^{\nu} \qquad \text{(C.12a)}$$

$$\Delta z = - \frac{H_0}{g^*} \; a_2 \; |\Delta T^*|^{\beta\delta} \; |1 - b_2^2 \; \theta^2|^{-\beta\delta} \; \theta(1-\theta^2) \qquad \text{(C.12b)}$$

The correlation length assumes its maximum value at the level $\Delta z = 0$ ($\theta = 0$) corresponding to the critical density. The height Δz_p at which the correlation length will be reduced by a factor $1-p$ is determined by the conditions

$$\theta_p = \pm \; b_2^{-1} \; [1 - (1-p)^{1/\nu}]^{1/2} \doteq \pm \; b_2^{-1} (\frac{p}{\nu})^{\frac{1}{2}} \qquad \text{(C.13)}$$

so that

$$\Delta z_p = - \frac{H_0}{g^*} \; \frac{a_2}{b_2} \; (\frac{p}{\nu})^{\frac{1}{2}} \; (\frac{\nu b_2^2 - p}{\nu b_2^2 - b_2^2 \beta\delta p}) \qquad \text{(C.14)}$$

$$\simeq - \frac{H_0}{g^*} \; \frac{a_2}{b_2} \; (\frac{p}{\nu})^{\frac{1}{2}} |\Delta T^*|^{\beta\delta}$$

The rate at which the correlation length ξ at arbitrary levels will vary as a function of height is determined by

81

$$\left(\frac{\partial c}{\partial z}\right)_T = \left(\frac{\partial \xi}{\partial \mu^*}\right)_T \left(\frac{\partial \mu^*}{\partial z}\right)_T = -\frac{g^*}{H_0} \; x_T^* \left(\frac{\partial \xi}{\partial c^*}\right)_T \qquad (C.15)$$

In terms of the parameters of the restricted cubic model this equation becomes

$$\left(\frac{\partial \xi}{\partial z}\right)_T = \left(\frac{g^*}{H_0}\right)\left(\frac{\xi_0}{a_2}\right) \quad r^{-(\gamma+2\delta)} \quad \left[\frac{2b_2^2 \theta}{2\beta\delta \, b_2^2 \, \mu^2(1-\theta^2)+(1-3\theta^2)(1-b_2^2\theta^2)}\right] \qquad (C.16)$$

in particular at the critical temperature $\Delta T^* = 0$, $(\theta = \pm \, b_2^{-1})$ this gradient will vary as

$$\left(\frac{\partial \xi}{\partial z}\right)_{T=T_c} = \pm \left(\frac{g^*}{H_0}\right)\left(\frac{\xi_0}{a_2}\right) \quad r^{-(\gamma+\beta\delta)} \; \frac{b_2^3}{\beta\delta(b_2^2-1)} \qquad (C.17a)$$

with $r(\Delta \mu^*)$ determined by

$$\Delta\mu^* = k_2 \; r^{\beta}(b_2^2 + c)/b_2^3 \qquad (C.17b)$$

The correlation length is the fundamental length scale which then determines the anomalous behavior of thermodynamic and transport properties near the critical point. In actual experiments these properties are measured as averages over a finite height h. Such experiments will be reliable when the correlation length over this height does not vary within the precision p desired. Thus in order to avoid errors due to gravity we require that

82

$$\left|\xi(\Delta z + h/2) - (\Delta z - h/2)\right| \le p\,\xi(\Delta z) \qquad (C.18)$$

which we approximate as

$$\frac{1}{\xi}\left(\frac{\partial \xi}{\partial z}\right)_T \le \frac{p}{h} \qquad (C.19)$$

Upon substituting (C.11a) and (C.16) into (C.19) we conclude that the errors due to gravity will become appreciable unless

$$r^{-\delta} \ge \left(\frac{g^+ h}{H_0 p}\right)\frac{1}{a_2}\left[\frac{2b_2^2\,\theta}{2\beta\delta\,b_2^2\theta\,(1-\theta^2)+(1-3\theta^2)(1-b_2^2\theta^2)}\right] \qquad (C.20)$$

When combined with (C.11b) and (C.11c) this equation defines a range in the $\Delta T^* - \Delta \rho^*$ plane where the measurements become inaccurate due to gravity effects. In particular at the critical temperature $\Delta T^* = 0$, this condition becomes

$$\ldots^* \ge \left(\frac{\gamma^+ h}{\rho H_0 D}\,\frac{1}{3\delta}\right)^{1/\delta} \qquad (C.21)$$

where D is the amplitude of the critical isotherm defined in (A.4d). In particular for xenon

$$|\Delta\rho^*| \geq 0.16 \left(\frac{g^*h}{p}\right)^{0.23} \tag{C.22}$$

where h is to be expressed in meters.

At the critical isochore $\Delta\rho^* = 0$ at $T \neq T_c$, $(\partial\xi/\partial z)_T = 0$ and (C.19) is not a good approximation to (C.18). The distance Δz_p over which the correlation length is reduced by a factor 1-p is given by (C.14). In order to avoid gravity effects we must require that this distance be larger than the height (strictly h/2) over which the properties are measured

$$\Delta z_p \geq \frac{h}{2} \tag{C.23}$$

It thus follows from (C.14) and (C.23) that at the critical isochore

$$|\Delta T^*| \geq \left[\frac{g^*h}{2H_o} \quad \frac{b_2}{d_2} \left(\frac{v}{p}\right)^{1/2}\right]^{1/\beta\delta} \tag{C.24}$$

In particular for xenon

$$|\Delta T^*| \geq 1.85 \times 10^{-3} \left(\frac{g^*h}{\sqrt{p}}\right)^{0.65} \tag{C.25}$$

where h is to be expressed in meters.

Table C.1. Critical Region Parameters for a Number of

Fluids Assuming Universal Effective Exponents

	Critical Point Parameters			Restricted Linear Model		Restricted Cubic Model		DH_0 *
	P_c MPa	ρ_c = kg/m³	T_c K	k_1	a_1	k_2	a_2	m
^{3}He	0.11678	41.45	-3.3099	0.924	4.58	0.818	4.05	906
^{4}He	0.22742	69.6	5.1895	1.021	6.40	C.904	5.66	946
Ar	4.865	535	150.725	1.309	16.1	1.160	14.2	2260
Kr	5.4931	908	209.286	1.309	16.1	1.16C	14.2	1500
Xe	5.8400	1110	289.734	1.309	16.1	1.160	14.2	1310
$p-H_2$	1.285	31.39	32.935	1.156	9.6	1.024	8.5	10410
N_2	3.398	313.9	126.24	1.361	18.2	1.206	16.1	2560
O_2	5.043	436.2	154.580	1.309	15.6	1.160	15.9	2790
H_2O	22.06	322.2	647.13	1.622	21.6	1.438	19.1	8980
D_2O	21.66	357	643.89	1.622	21.6	1.438	19.1	7950
CO_2	7.3753	467.8	304.127	1.436	21.3	1.273	18.9	3470
NH_3	11.303	235	405.4	1.573	21.4	1.394	19.1	7134
SF_6	3.7605	730	318.687	1.337	23.9	1.185	21.2	1730
CH_4	4.595	162.7	190.555	1.361	17.0	1.206	15.1	6260
C_2H_4	5.0390	215	282.344	1.350	17.5	1.197	15.5	5540
C_2H_6	4.8718	206.5	30 .33	1.416	20.2	1.255	17.9	5520
C_3H_8	4.247	221	369.82	1.451	20.2	1.286	17.9	3830

Notes: $\alpha = 0.100$ $\beta = 0.355$

$\gamma = 1.190$ $\delta = 4.352$ $b_1^2 = 1.3909$ $b_2^2 = 1.3100$ $c = 0.0393$

$\nu = 0.633$ $\eta = 0.12$

*The last quantity tabulated, $DH_0 = D P_c /(\rho_c \, mg_n)$ is the scale factor for the density vs height profile at the critical temperature. D is found from the relation:
$D = a_1 k_1^{-\delta} b_1^{\delta-3} (b_1^2 - 1)$, which is taken from Sengers et al. [1976].

Appendix D. Physical constants for various fluids.

In this Appendix we present critical parameters and critical region parameters for a number of fluids, taken from a survey prepared by Sengers and Levelt Sengers [1977]. The restricted linear model and cubic model parameters in this table represent informed estimates assuming universal effective critical experiments corresponding to the range

$$5\times10^{-4} \leq |\Delta T^*| \leq 3\times10^{-2}, \qquad |\Delta\rho^*| \leq 0.25 \qquad (D.1)$$

Appendix E. Parameters used for xenon in this report.

Critical point parameters (Levelt Sengers et al., 1976)

$$P_c = 5.8400 \text{ MPa}$$

$$m\rho_c = 1110 \text{ kg/m}^3$$

$$T_c = 289.734 \text{ K}$$

$$H_o = P_c/\rho_c g_o = 536 \text{ m}$$

Restricted linear model (Levelt Sengers et al., 1976)

$\alpha = 0.100$	$A = 1.71$	$k_1 = 1.309$
$\beta = 0.355$	$B = 1.827$	$a_1 = 16.1$
$\gamma = 1.19$	$\Gamma = 0.0813$	$b_1^2 = 1.3909$
$\delta = 4.352$	$D = 2.44$	

Restricted cubic model (Sengers and Levelt Sengers, 1976)

$\alpha = 0.100$	$A = 1.68$	$k_2 = 1.160$
$\beta = 0.355$	$B = 1.827$	$a_2 = 14.2$
$\gamma = 1.19$	$\Gamma = 0.0817$	$b_2^2 = 1.3100$
$\delta = 4.352$	$D = 2.44$	$c = 0.0393$

Wilcox-Estler model (Hocken and Moldover, 1976)

$n_c = 1.1379$	$\beta = 0.3293$	$\theta_o = 0.1076$
$n_c' = 0.14$	$\gamma = 1.229$	$Y_o^\beta = 0.323$
	$\Delta = 4.4$	

Correlation length (Swinney and Henry, 1973)

$$\nu = 0.633 \qquad \xi_o = 2.0 \times 10^{-10} \text{ m}.$$

Acknowledgments

Nomenclature

A = amplitude of power law for specific heat C_v

a_1 = parameter of linear model

a_2 = parameter of cubic model

B = amplitude of power law for coexistence curve

b_1 = parameter of linear model

b_2 = parameter of cubic model

C_v = constant-volume heat capacity

C_v^* = $C_v T_c / V_c P_c$

c = parameter of cubic model

D = amplitude of power law for chemical potential along critical isotherm

d = sample thickness

$g(R)$ = correlation function as a function of distance

g = gravitational acceleration

g_o = 9.80 m/s^2 = earth's gravitational acceleration (units)

g^* = g/g_o = gravitation acceleration relative to its value at the earth's surface

h = sample height

H = $P_c/\rho_c mg$ = scale height for chemical potential

H_o = $P_c/\rho_c mg_o$ ′ scale height for chemical potential on earth

k = wave ve. r

K_T = $\rho^{-1}(\partial\rho/\partial P)_T$ = isothermal compressibility

k_B = Boltzmann's constant

k_1 = parameter of linear model

k_2 = parameter of cubic model

m = molecular mass

n = refractive index

89

n_c = refractive index at critical point

n_1 = $(\partial n / \partial \rho *)_T$

n_c^1 = n_c^1 = value of n_1 at critical point

P = Pressure

P_c = critical pressure

$P*$ = P/P_c

$\Delta P*$ = $(P-P_c)/P_c$

p = desired precision

r = parametric variable

$\vec{R}$ = spatial coordinate

R = magnitude of spatial coordinate

$\hat{R}$ = scaling function for correlation length (Appendix C.2)

S = structure factor

T = temperature in Kelvin

T_c = critical temperature

$T*$ = T/T_c

$\Delta T*$ = $(T-T_c)/T_c$

t = $\Delta T*$

V = volume

x = scaled thermodynamic variable $\Delta T*/|\Delta \rho *|^{1/\beta}$ or scaled wave vector $k\xi$

x_o = $B^{-1/\beta}$

Y_o = parameter of Wilcox-Estler model

z = height

z_o = height at which $\rho = \rho_c$

Δz = $z-z_o$

Greek letters

α = exponent of power law for specific heat C_v

β = exponent of power law for coexistence curve

γ = exponent of power law for compressibility χ_T

Γ = amplitude of power law for compressibility χ_T

Γ_s = decay rate of entropy fluctuations

δ = exponent of power law for chemical potential along critical isotherm

ϵ = dielectric constant

$\Delta = 1 - \theta_o/\theta_x$ = parameter of Wilcox-Estler model

η = exponent for spatial dependence of correlation function at the critical point

θ = parametric variable

θ_o = value of θ on critical isochore in Wilcox-Estler model

θ_x = value of θ on coexistence curve in Wilcox-Estler model

ξ = correlation length

ξ_o = amplitude of power law for correlation length

λ = wave length

μ = chemical potential per particle

μ^* = $\mu \rho_c/P_c$

$\Delta\mu^*$ = $\{\mu(\rho,T) - \mu(\rho_c,T)\}\rho_c/P_c$

ν = exponent of power law for correlation length

ρ = number density

ρ_c = critical density (particles/volume)

$\bar{\rho}$ = average density

ρ^* = ρ/ρ_c

$\Delta\rho^*$ = $(\rho - \rho_c)/\rho_c$

91

ρ_{cxc} = density of vapor or liquid at coexistence

ρ_{cxc}^{*} = ρ_{cxc}/ρ_c

$\Delta\rho_{cxc}^{*}$ = $(\rho_{cxc} - \rho_c)/\rho_c$

σ = cross section area

τ = turbidity

χ_T = $(\partial\rho/\partial\mu)_T = \rho^2 K_T$

χ_T^{*} = $(\partial\rho^*/\partial\mu^*) = \chi_T P_c/\rho_c^2$

ω = frequency

92

References.

1. Balzarini, D. and K. Ohrn, 1972, Phys. Rev. Letters, $\underline{29}$, 814.

2. Bedeaux, D. and P. Mazur, 1973, Physica $\underline{67}$, 23.

3. Born, M. and E. Wolf, 1975, "Optics", Pergamon Press. The ray
   tracing equations appear in many other places as well.

4. Bray, A.J. and R.F. Chang, 1975, Phys. Rev. $\underline{A12}$, 2594.

5. Brown, G.R. and H. Meyer, 1972, Phys. Rev. $\underline{A6}$, 364.

6. Cahn, J.W., 1968, Trans. AIME $\underline{242}$, 16.

7. Cannell, D.S., 1975, Phys. Rev. $\underline{A12}$, 225.

8. Chu, B. 1972, Ber. Bunsenges. physik Chemie $\underline{76}$, 202.

9. Cummins, H.Z. and H.L. Swinney, 1970, in "Progress in Optics",
   Vol. 8, E. Wolf, ed. (North-Holland, Amsterdam), Ch. 3.

10. Dahl, D. and M.R. Moldover, 1972, Phys. Rev. $\underline{A6}$, 1915.

11. D'Arrigo, G., L. Mistura, and P. Tartaglia, 1975, Phys. Rev.
    $\underline{A12}$, 2587.

12. Dodge, F.T., H.N. Abramson, S.W. Angrist, I. Catton, S.W. Churchill,
    R.J. Mannheimer, S.Ostrach, S.H. Schwartz, and J.V. Sengers, 1975,
    "Fluid Physics, Thermodynamics, and Heat Transfer Experiments in
    Space: Final Report of the Overstudy Committee", NASA Contractor
    Report No. NASA CR-134742, NASA Lewis Research Center,
    Cleveland, Ohio, 44135.
    Edwards, M.H. and W.C. Woodbury, 1963, Phys. Rev. $\underline{129}$, 1911.

13. Elcock, E.W., 1956, Order-Disorder Phenomena (John Wiley,
    New York, 1956).

14. Estler, W.T., R. Hocken, T. Charlton and L.R. Wilcox, 1975,
    Phys. Rev. $\underline{A12}$, 2118.

15. Fisher, M.E., 1964, J. Math. Phys. $\underline{5}$, 944.

16. Fisher, M.E., 1967, Reports on Progress in Physics $\underline{30}$ (II), 615.

17. Giglio, M. and A. Vendramini, 1975, Phys. Rev. Lett. $\underline{35}$, 168.

93

18. Greer, S.C., M.R. Moldover and R. Hocken, 1974, Rev. Sci. Instrum., 45, 1462.

19. Greer, S.C., T.E. Block and C.M. Knobler, 1975, Phys. Rev. Lett. 34, 250.

20. Griffiths, R.B., 1967, Phys. Rev. 158, 176.

21. Griffiths, R.B. and J.C. Wheeler, 1970, Phys. Rev. A2, 1047.

22. Hartley, C.L., D.T. Jacobs, R.C. Mockler and W.J. O'Sullivan, 1974, Phys. Rev. Letters 33, 1129.

23. Heller, P., 1967, Reports on Progress in Physics 30 (II), 737.

24. Ho, J.T. and J.D. Litster, 1970, Phys. Rev. B2, 4523.

25. Hocken, R. and M.R. Moldover, 1976, Phys. Rev. Lett. 37, 29.

26. Hocken, R. and G. Stell, 1973, Phys. Rev. A8, 887.

27. Hocken, R., M.R. Moldover, E. Muth and S. Gerner, 1975, Rev. Sci. Instr. 46, 1699.

28. Hohenberg, P.C. and M. Barmatz, 1972, Phys. Rev. A6, 289.

29. Huang, C.C. and J.T. Ho, 1973, Phys. Rev. A304.

30. Huang, J.S., W.I. Goldburg and M.R. Moldover, 1975, Phys. Rev. Lett. 34, 639.

31. Josephson, B.D., 1969, J. Phys. C2, 1113.

32. Kadanoff, L.P., 1966, Physics 2, 263.

33. Kim, D.M., D.L. Henry and R. Kobayashi, 1974, Phys. Rev. A10, 1808.

34. Langer, J.S. and M. Bar-on, Ann. Phys. (N.Y.) 78, 421.

35. Larson, S.Y., R.D. Mountain and R. Zwanzig, 1965, J. Chem. Phys. 42, 2187.

36. Leung, H.K. and B.N. Miller, 1975, Phys. Rev. A12, 2163

37. Leung, S.S. and R.B. Griffiths, 1973, Phys. Rev. A8, 2670.

38. Levelt Sengers, J.M.H., 1974, Physica 73, 73.

39. Levelt Sengers, J.M.H., 1975, in "Experimental Thermodynamics" Vol. II., B. LeNeindre and B. Vodar, eds. (Butterworth, London).

40. Levelt Sengers, J.M.H., W.L. Greer and J.V. Sengers, 1976, J. Phys. Chem. Ref. Data $\underline{5}$, 1.

41. Levelt Sengers, J.M.H. and J.V. Sengers, 1975, Phys. Rev. $\underline{A12}$, 2622.

42. Lin, J.S. and P.W. Schmidt, 1974, Phys. Rev. $\underline{A10}$, 2290.

43. Lorentz, H.A., 1952, "Theory of Electrons", 2nd. ed., Dover, New York.

44. Lorentzen, H.L. and B.B. Hansen, 1966, in "Critical Phenomena", N.B.S. Miscellaneous Publ. 273, (Eds.) M.S. Greer and J.V. Sengers (U.S. Govt. Printing Office, Washington, D.C.), p. 213.

45. Lorenz, L., 1880, Ann. Phys. Chem. $\underline{11}$.

46. Ma, S., 1973, Rev. Mod. Phys. $\underline{45}$, 589.

47. Murphy, T.A., J.V. Sengers and J.M.H. Levelt Sengers 1973, in Proc. 6th Symposium on Thermophysical Properties, P.E. Liley, ed. (American Society of Mechanical Engineers, New York), p. 180.

48. Murphy, T.A., J.V. Sengers and J.M.H. Levelt Sengers, 1975, in Proc. 8th Intern. Conf. on Properties of Water and Steam, P. Bury, h. Perdon and B. Vodar, eds. (Editions Europeennes Thermoques et Industries, Paris). p. 603.

49. Puglielli. V.G. and N.C. Ford, 1970, Phys. Rev. Letters, $\underline{25}$, 143.

50. Reith, L.A. and H.L. Swinney, 1975, Phys. Rev. $\underline{A12}$, 1096.

51. Rowlinson, J.S., 1969, "Liquids and Liquid Mixtures". 2nd. ed. (Butterworth, London).

52. Schmidt, H.H., 1971, J. Chem. Phys. $\underline{54}$, 3610.

53. Schofield, P., 1969, Phys. Rev. Letters $\underline{22}$, 606.

54. Schofield, P., J.D. Litster and J.T. Ho, 1969, Phys. Rev. letters $\underline{23}$, 1098.

55. Schwartz, A.J., J.S. Huang and W.I. Goldburg, 1975, J. Chem. Phys. 62, 1847.

56. Sengers, J.V., 1973 in "Transport Phenomena-1973", J. Kestin, editor AIP Conference Proceedings Number 11 (American Institute of Physics, New York), p. 229.

57. Sengers, J.V. and J.M.H. Levelt Sengers, 1977, in "Progress in Liquid Physics", C.A. Croxton, ed. (Wiley, New York), Ch. 5.

58. Stanley, H.E., 1971, "Introduction to Phase Transitions and Critical Phenomena" (Oxford Univ. Press. New York).
Splittorff, O. and B.N. Miller, 1974, Phys. Rev. 9, 550.

59. Stell, G. and J.S. Hoye, 1974, Phys. Rev. Letters 33, 1268.

60. Swinney, H.L. and O.L. Henry, 1973, Phys. Rev. A8, 2586.

61. Thoen, J. and C.W. Garland, 1974, Phys. Rev. A10, 1311.

62. Tracy, C.A. and B.M. McCoy, 1975, Phys. Rev. B12, 368.

63. Vicentini-Missoni, M., J.M.H. Levelt Sengers and M.S. Green, 1969, J. Res. Natl. Bur. Stand. (U.S.) 73A, 563.

64. Warkulwiz, V.P., B. Mozer and M.S. Green, 1974, Phys. Rev. Lett. 32, 1410.

65. Weber, L.A., 1970, Phys. Rev. A2, 2379.

66. Weiner, J., J.H. Langley and N.C. Ford, Jr., 1974, Phys. Rev. Lett. 32, 879.

67. White, J.A. and B.S. Maccabee, 1975, Phys. Rev. A11, 1706.

68. Widom, B., 1965, J. Chem. Phys. 43, 3898.

69. Widom, B., 1964, Physica 73, 107.

70. Wilcox, L.R. and W.T.Estler, 1971, Journal de Physique (Paris), Colloque CSa, Supplement. au No. 10, 32, 175.

71. Wilson, K.G. and J. Kogut, 1974, Phys. Rep. 12C, 75.